AFOSR-TR- 79-0021

Final Scientific Report

Contract F49620–77–C–0077

LEVEL II

BUCKLING OF CONTINUOUS FILAMENT ADVANCED COMPOSITE ISOGRID WIDE COLUMNS IN AXIAL COMPRESSION

By

Lawrence W. Rehfield and Ravi B. Deo

November 1978

GEORGIA INSTITUTE OF TECHNOLOGY
SCHOOL OF AEROSPACE ENGINEERING
ATLANTA, GEORGIA 30332

1978

BUCKLING OF CONTINUOUS FILAMENT ADVANCED COMPOSITE ISOGRID WIDE COLUMNS IN AXIAL COMPRESSION

Final Scientific Report
AFOSR Contract F49620-77-C-0077

Lawrence W. Rehfield[1] and Ravi B. Deo[2]
School of Aerospace Engineering
Georgia Institute of Technology
Atlanta, Georgia 30332

1. Professor.

2. Assistant Research Engineer.

UNCLASSIFIED
SECURITY CLASSIFICATION OF THIS PAGE (When Data Entered)

REPORT DOCUMENTATION PAGE

READ INSTRUCTIONS BEFORE COMPLETING FORM

1. REPORT NUMBER: AFOSR-TR-79-0021	2. GOVT ACCESSION NO.
3. RECIPIENT'S CATALOG NUMBER	
4. TITLE (and Subtitle): BUCKLING OF CONTINUOUS FILAMENT ADVANCED COMPOSITE ISOGRID WIDE COLUMNS IN AXIAL COMPRESSION.	5. TYPE OF REPORT & PERIOD COVERED: FINAL SCIENTIFIC rept. 1 March 1977 — 30 June 1978
	6. PERFORMING ORG. REPORT NUMBER
7. AUTHOR(s): Lawrence W. Rehfield and Ravi B. Deo	8. CONTRACT OR GRANT NUMBER(s): F49620-77-C-0077
9. PERFORMING ORGANIZATION NAME AND ADDRESS: Georgia Institute of Technology, Aerospace Engineering, Atlanta, Georgia 30332	10. PROGRAM ELEMENT, PROJECT, TASK AREA & WORK UNIT NUMBERS: 2307 B1, 61102 F
11. CONTROLLING OFFICE NAME AND ADDRESS: AF Office of Scientific Research (NA), Building 410, Bolling AFB, D. C. 20332	12. REPORT DATE: November 1978
	13. NUMBER OF PAGES: 61
14. MONITORING AGENCY NAME & ADDRESS (if different from Controlling Office): 65 p.	15. SECURITY CLASS. (of this report): UNCLASSIFIED
	15a. DECLASSIFICATION/DOWNGRADING SCHEDULE

16. DISTRIBUTION STATEMENT (of this Report)

Approved for Public Release
Distribution Unlimited

17. DISTRIBUTION STATEMENT (of the abstract entered in Block 20, if different from Report)

18. SUPPLEMENTARY NOTES

19. KEY WORDS (Continue on reverse side if necessary and identify by block number)

Buckling, Composites, Isogrid

20. ABSTRACT (Continue on reverse side if necessary and identify by block number)

This report contains a summary of research performed to explore the potential of a new, promising structural concept---continuous filament advanced composite isogrid. This is the first attempt to evaluate it in load bearing structure. A data base has been established by the design, fabrication and test of flat panels as wide columns. Correlation of the experimental results with theory, on a relative basis, is excellent. Inconsistency in manufacturing is clearly identified as the major reason for scatter in observed data, a problem which would not exist in a production environment. The results presented

DD FORM 1 JAN 73 1473 EDITION OF 1 NOV 65 IS OBSOLETE

UNCLASSIFIED (over)
SECURITY CLASSIFICATION OF THIS PAGE (When Data Entered)

403 914

are a major step toward inspiring the necessary confidence in the use of this concept in airframe structure.

ABSTRACT

This report contains a summary of research performed to explore the potential of a new, promising structural concept---continuous filament advanced composite isogrid. This is the first attempt to evaluate it in load bearing structure. A data base has been established by the design, fabrication and test of flat panels as wide columns. Correlation of the experimental results with theory, on a relative basis, is excellent. Inconsistency in manufacturing is clearly identified as the major reason for scatter in observed data, a problem which would not exist in a production environment. The results presented are a major step toward inspiring the necessary confidence in the use of this concept in airframe structure.

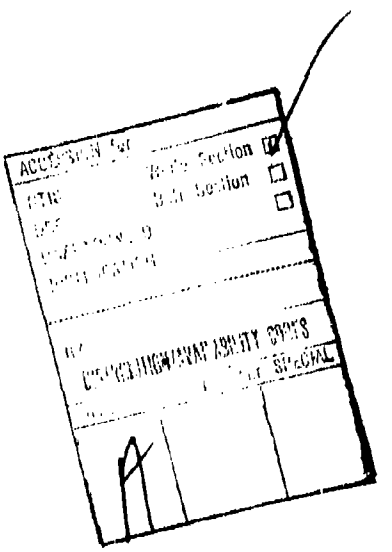

INTRODUCTION

Preliminary Remarks

This report contains a summary of research sponsored by the United States Air Force Office of Scientific Research under Contract F49620-77-C-0077, "Behavior of Advanced Composite Isogrid Structures." This project is a cooperative effort between the Georgia Institute of Technology (GIT) and McDonnell Douglas Astronautics Company - East (MDAC-E). Professor Lawrence W. Rehfield is the Principal Investigator and directly supervised the portion of the work performed at the School of Aerospace Engineering, GIT. Mr. Ramon A. Garrett provided technical supervision for the work performed at MDAC-E. All work was performed during the period 1 March 1977 to 30 June 1978.

The Isogrid Stiffening Concept

The search for efficient, light-weight aerospace vehicle structural concepts is a continuing process. Major airframe components are normally plate - or shell-type structures. Efficiency dictates that they be stiffened or semi-monocoque in construction. The usual means of stiffening is to use longitudinal stringers and frames or ribs which are orthogonal to the stringers or nearly so. This type of construction has several distinct advantages, which include the following:

(1) it possesses a high stiffness to weight ratio for efficiency;

(2) stiffening results in high effective bending stiffness for circumventing local flutter, vibration and buckling problems;

(3) stiffening members are useful for attachment of secondary structure and non-structural items and for the introduction of concentrated or localized loads; and

(4) cutouts for access doors and windows are easily incorporated into the design.

An alternative approach to stiffening which also possesses these advantages is isogrid.

Isogrid is a stiffening concept that employs a repetitive equilateral triangular pattern of ribs. It was developed by Dr. Robert R. Meyer of McDonnell Douglas Astronautics Company-West in 1964 under NASA contract. The name "isogrid" refers to the fact that the triangular grid behaves in a gross sense as an isotropic material. Unlike orthogonal stiffener grids, isogrid is a stable configuration by itself and may be used with or without attached skin. (Only isogrid with skin is considered here, however.) It has been successfully employed in metallic, integrally stiffened form to spacecraft tankage and interstages[1,2] and in the Skylab crew quarters.[1] The overall isogrid geometric configuration is shown in Figure 1.

In addition to the advantages listed previously for stiffened shell construction, isogrid possesses three more important ones:

(1) because it is effectively isotropic, many existing analytical solutions can be adapted directly for use in design[1];

(2) the nodes formed by intersecting triangles can be used very effectively as attach points and for diffusing concentrated loads;

(3) if the isogrid is made separately from the skin and then assembled to it, a crack in either lattice or skin cannot be propagated across the joint.[1] (This is also true of other bonded structures.)

Naturally, there will be some applications where a slight weight penalty may be associated with isogrid's uniformity of configuration and isotropic stiffening. It may still be the concept of choice, however, when evaluated in the total context because of cost factors. Isogrid panels, for example, can be produced in large quantities and utilized as modular construction units in a variety of applications.

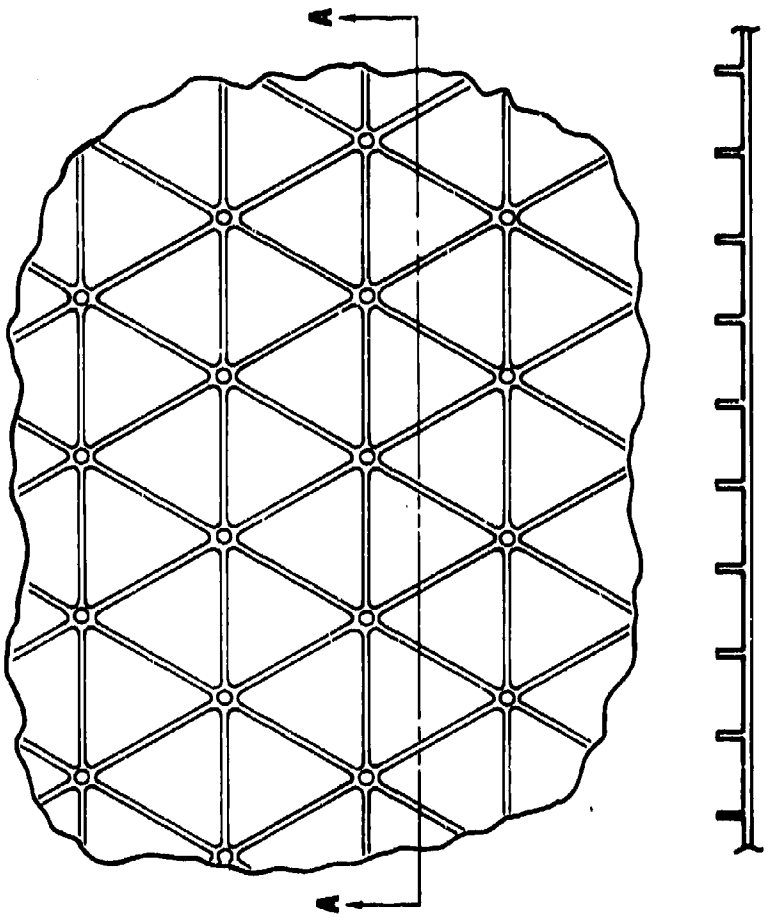

FIGURE 1. ISOGRID GEOMETRIC CONFIGURATION

Continuous Filament Advanced Composite Isogrid

High expectations are held for composite materials. New design concepts employing these materials are predicted to improve system performance, lower the structural fraction of total system weight (15-25 percent according to some estimates) and reduce total life cycle costs. Composites are generally recognized as the primary materials for the next generation of aerospace vechicles. There are difficulties that must be overcome in order for these expectations to be realized, however. Among the most important are

(1) continuing high material and manufacturing costs,

(2) lack of service experience and proven nondestructive inspection (NDI) techniques, and

(3) uncertainties associated with long-term and severe environmental effects (for resin matrix materials systems).

An advanced composite isogrid has been developed by McDonnell Douglas Astronautics Company-East (MDAC-E) that is intended to be structurally efficient while overcoming the major difficulty of high manufacturing costs.

The development of the MDAC-E advanced composite isogrid has been a company-funded manufacturing technology program which began approximately four years ago. The latest manufacturing innovation is based upon the use of weaving and braiding techniques first developed in the textile and garment industry. The new process consists of weaving or braiding prepreg tape or yarn continuously around a mandrel-like tool to produce a seamless fabric with the shape of the tool. The resulting fabric or mat is then subsequently cured. This process is economical because it is automated. It results in a high quality, seamless composite that is uniform from part to part. Furthermore, weaving or braiding over a variety of shapes is possible, including surfaces with compound curvature.

In order to manufacture composite isogrid by this process, a tool must be made that defines the triangular rib pattern. The "backbones" for the ribs are

constructed of essentially continuous unidirectional fibers by use of a weaving process (for flat structures) or braiding (for cylindrical or curved structures). The tool acts as both a loom and a mold for impregnating the fibers with resin and curing the composite in the desired isogrid pattern. Skin can be co-cured with the isogrid lattice or bonded to it at a later time in a separate operation. By virtue of the fact that the grid or lattice is a continuous filament structure, the result is called continuous filament advanced composite isogrid (CFACI).*

CFACI possesses all the benefits of isogrid-type stiffening. In addition, it holds the promise of weight-savings and superior performance of a composite. Another factor which is of considerable practical importance is the potential for completely automating the manufacturing process. This would impact two major problems normally associated with composite structures---high initial cost and uniformity of product. For the potential of CFACI to be realized, basic data on load bearing structure must be acquired and evaluated in conjunction with current theoretical models and analysis methods; this is the task that has begun under this contract.

---

*Another advanced composite isogrid has been developed by McDonnell Douglas Astronautics Company-West based upon another manufacturing process.[3] This isogrid is epoxy reinforced with unidirectionally aligned chopped graphite fibers formed by compression molding. It is not a continuous filament structure, therefore.

PROJECT OVERVIEW

Objectives

The objectives of this research are

(1) to investigate the adequacy of existing design analysis methods for predicting the behavior of CFACI structural elements;

(2) to establish a data base for inspiring confidence in the use of CFACI in applications and for correlation of experimental results with existing theory; and

(3) to identify and define problem areas where the state-of-the-art in design analysis and manufacture of CFACI must be advanced.

These objectives are best met by a broad-based program that includes design, manufacture, and experimental evaluation of structural components of increasing complexity and concomitant correlation of the data obtained with the design analysis predictions. The first phase of such a program has been completed.

Division of Effort

CFACI as it evolved was an interesting structural concept, but untried in load bearing structure. Basic information was needed. The program of research that has been pursued synergistically combines the capability and experience of GIT in basic structural research with that of MDAC-E in design and manufacture. By virtue of the basic nature of the work, GIT is the prime contractor. MDAC-E, as subcontractor, has been responsible for tooling, manufacturing, quality control and state-of-the-art design analysis. The basic structural experiments and correlation studies have been done by GIT.

Scope

Because isogrid is a stiffening concept, it is natural to consider stiffness critical applications. One of the most practically important, simple contexts is buckling under uniaxial compression. This is the first condition that has been

studied for wide columns and circular cylindrical shells.

The first phase of the work that is described herein can be summarized as follows:

(1) Existing isogrid analysis methods[1] and MDAC-E proprietary computer programs were used to design a wide column structure and a stiffened cylindrical shell by state-of-the-art design techniques.

(2) Three nominally identical wide columns were manufactured by MDAC-E according to the above design.

(3) The wide columns have been experimentally evaluated in compression by GIT and the observed behavior compared with the design predictions.

In addition, a number of supporting element tests have been performed which add pertinent information to the data base; these will be described in a separate report.

Rationale

Much of the existing metallic isogrid is found in stiffness critical structure designed to resist buckling. Consequently, the simplest structure of this type, a wide column, is the logical choice for the first CFACI evaluation. The wide column poses most of the design challenges normally encountered, such as secondary modes of instability (skin buckling and rib crippling), without introducing the difficulties associated with intrinsic imperfection sensitivity. All issues pertaining to optimum proportioning must be considered also. Since the wide column is a flat structure and three nominally identical ones were built, problems arising from manufacturing CFACI by flat weaving have been identified. Uniformity from part to part that can be achieved by current manufacturing methods is a prime concern.

A thorough design analysis for a compressed cylindrical shell, in addition to providing valuable experience, set the stage for future work at the next level of complexity and challenge. If sufficient promise is demonstrated in the first phase, manufacture and evaluation of cylindrical shells is the next

logical step to take in extending the CFACI technology base. Problems associated with manufacturing by braiding would be uncovered, while the impact of imperfection sensitivity would become evident.

DESIGN ANALYSIS

Design Constraints

There was considerable flexibility in the choice of configurations for the wide column panels and the cylindrical shells. The constraints imposed upon the designs were:

(1) the mode of buckling should be general instability and should occur at a total compressive load less than 100,000 pounds;

(2) the buckling mode should have a number of waves along the length of the structure;

(3) the structures should be of realistic size that reflects both potential applications and compatibility with existing test facilities in GIT's Aerospace Structures Laboratory; and

(4) the mean compressive buckling strains for both the wide columns and the shells are the same.

Items (1) and (3) are related to the load producing capacity and test bed dimensions of the Baldwin testing machine used for the experiments. Contraint (2) was imposed in order to minimize the influence of boundary restraint on the buckling behavior; boundary restraint effects, although quite important, are not the main issues under investigation. Contraint (4) permits the maximum degree of applicability of the panel data to the shells and reduces the risk associated with unanticipated modes of failure in a future shell program.

A diameter of 20 inches was preselected for the cylindrical shell design study; this is a size that is manageable and representative of tactical missile applications. Also, the material system was selected on the basis of prior manufacturing experience at the McDonnell Douglas St. Louis facility. While a definite length for the cylinders was not preselected, 36 inches was the maximum considered.

Material Selection

The graphite/epoxy material system selected utilizes Union Carbide T300 continuous graphite filaments in a DeSoto Company 1848-114 epoxy matrix. It is available as 1/4 inch wide prepreg tape for use in braiding the isogrid skin. The T300 fiber system was selected because of its high strength, relatively high modulus and the ease with which it can be braided. The 1848-114 resin system is formulated for graphite fiber reinforcement in prepreg braiding applications. It is a short cure type 350°F system which will completely cure in 20 minutes, has a 350°F gel time of six minutes and a volatile content of less than one percent.

Typical T300 graphite fiber properties are given in Table 1. For design purposes, the resin was assumed to have a modulus of 350,000 psi and a Poisson's ratio of 0.33. The fiber volume fraction was assumed to be 0.60.

The grid rib lattice for the flat panels was woven from T300 prepreg yarn that has a 0.019 inch diameter containing 3000 filaments. The skin is quasi-isotropic; it was braided to a $[0, \pm 60]$ configuration. In the 0° direction (along the longitudinal axis of the panels), the prepreg tapes contain 30,000 filaments. Tapes in the $\pm 60^{\circ}$ directions were more closely spaced as they contain 15,000 filaments. Estimated room temperature properties used in the design analysis are summarized in Table 2. The skin modulus was based on predictions using classical lamination theory. Strengths were conservatively estimated based upon experience with similar composite material systems.

Design Analysis Methodology

The design of stiffened plates and shells to resist buckling is facilitated by considering three limiting types of buckling modes. They are rib crippling, skin buckling and general instability. Each mode is assumed to be independent and distinct in a buckle resistant design. They are illustrated in Figure 2.

An intuitive design approach that, although it is not rigorous or always.

FIBER PROPERTIES	
TENSILE STRENGTH	360×10^3 LBS/IN^2
TENSILE MODULUS	34×10^6 LBS/IN^2
ULTIMATE ELONGATION	1.1%
DENSITY	0.063 LBS/IN^3
YARN/TOW CHARACTERISTICS	
FILAMENT SHAPE	ROUND
FILAMENT COUNT	3000
TWIST	0.4 TURNS/IN
FILAMENT DIAMETER	2.72×10^{-4} IN
YARN CROSS SECTION AREA	17.43×10^{-5} IN^2

TABLE 1. TYPICAL T300 GRAPHITE FIBER AND YARN PROPERTIES

PROPERTY \ ITEM	RIB	SKIN
TENSILE STRENGTH (PSI)	188,000	54,000
COMPRESSIVE STRENGTH (PSI)	188,000	54,000
INTERLAMINAR SHEAR STRENGTH (PSI)	14,000	14,000
YOUNGS MODULUS (MSI)	20.4	8.0
DENSITY (LB/IN^3)	0.056	0.056

TABLE 2. ESTIMATED COMPOSITE PROPERTIES

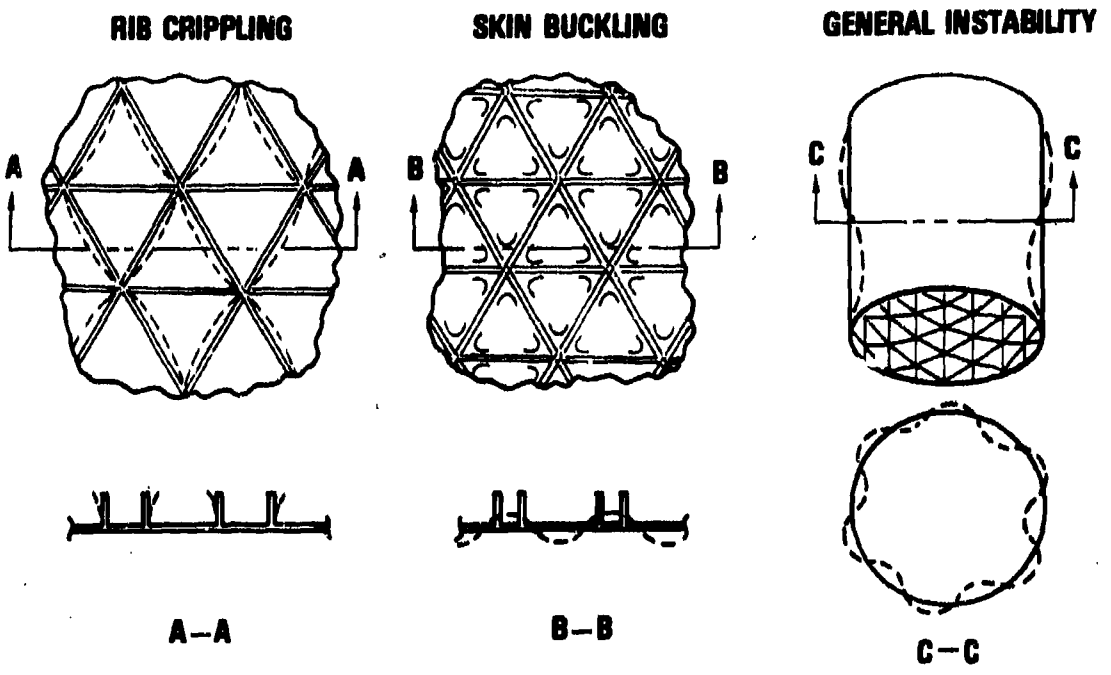

FIGURE 2. RIB, SKIN AND GENERAL INSTABILITY BUCKLING MODES

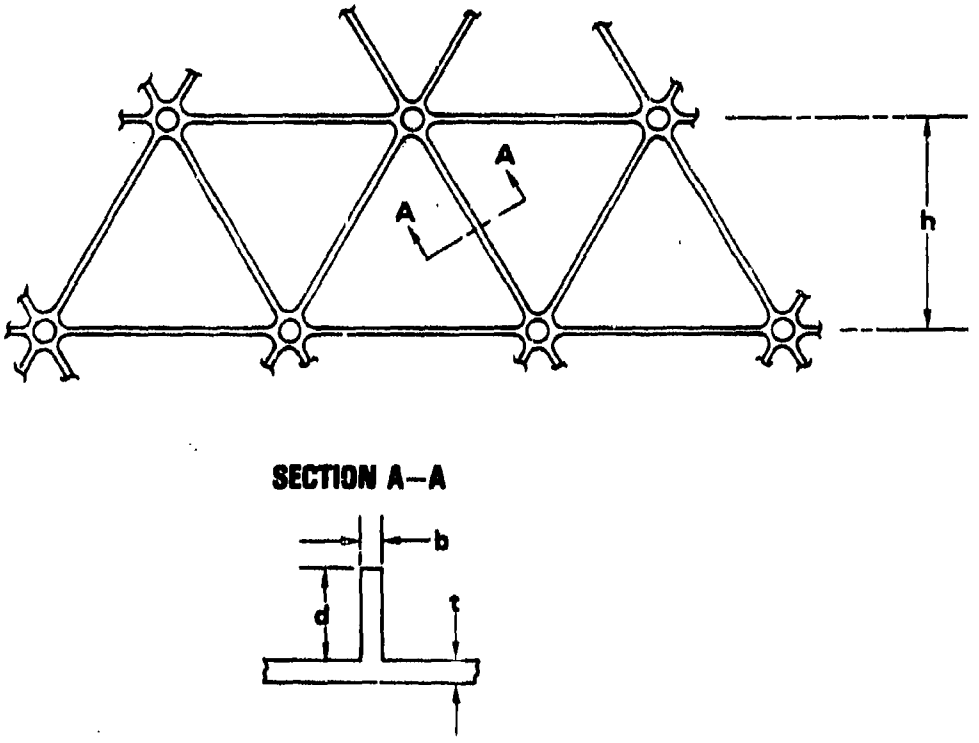

FIGURE 3. ISOGRID GEOMETRY

reliable, has often been used in the past is the simultaneous mode design (SMD) method. The premise upon which the SMD method is based is the assumption that the optimum (least weight) design results if all failure modes occur simultaneously. This is not always a valid assumption. Furthermore, this assumption can result in buckle resistant designs that are far from optimum in a practical sense; the reason for this is that nonlinear modal interactions can be present that render an SMD based upon independent, distinct failure modes highly sensitive to imperfections. The optimization studies of isogrid structures presented in Reference 1 are all based upon the SMD method. Consequently, while some of the analysis methods given in Reference 1 have been used, the design methods have not.

Isogrid, by definition, is a stiffening concept that yields a structure which is effectively isotropic in a gross sense. The methods of analysis for predicting some of the modes of buckling, therefore, are modifications of known results applicable to unstiffened structures made of isotropic materials. Many of these are presented in Reference 1 for isogrid structures made of isotropic materials. The methods are modified for structures with distinct skin and rib properties in Reference 2. The results applicable to CFACI construction are summarized in the sequel; these were used in the design analysis.

Local crippling of the ribs and skin buckling differ substantially from general instability in terms of practical consequences for compressed stiffened cylindrical shells. The former types of buckling do not, or at least need not, precipitate total collapse of the cylinder. In fact, designs that permit some degree of elastic postbuckling deformation in these modes may be tolerated in service for some applications. General instability involves the complete structure, however. It almost always corresponds to total collapse

and is usually accompanied or closely followed by substantial permanent damage. General instability is the major influence on the cylinder design, therefore. For this reason, the cylindrical shells and wide columns were designed to buckle in the general instability mode.

Isogrid geometry and associated parameters are defined in Figure 3. General instability for CFACI compressed cylindrical shells was analyzed using two levels of sophistication. The preliminary design analysis that was used for trade studies was based upon the following equation from Reference 2:

$$N_{CR} = C_o E_o \frac{t^2}{R} \bar{\beta} \tag{1}$$

N_{CR} is the value of compressive stress resultant to cause buckling, E_o is the elastic modulus of the skin, t is the skin thickness and R is the shell radius of the skin midsurface. C_o was taken to be 0.397 as recommended in Reference 1; this is the result of applying a "knockdown" factor of 0.65 to the classical buckling formula. (This knockdown is recommended by Peterson[4] after studying experimental data on tests of stiffened, metallic cylinders.) $\bar{\beta}$ is defined by

$$\bar{\beta} = \left[3\bar{\alpha}\,(1+\delta)^2 + (1+\bar{\alpha})\,(1+\bar{\alpha}\,\delta^2)\right]^{1/2} \tag{2}$$

where

$$\bar{\alpha} = \frac{\bar{b}d}{th}\,,\quad \bar{b} = b\,\frac{E_1}{E_0}\,,\quad \delta = \frac{d}{t} \tag{3}$$

b is the rib width, d is the rib depth and h is the height of the triangular pattern of ribs. E_1 is the elastic modulus of the ribs.

Skin buckling was predicted on the basis of the following equation:

$$N_{CR} = C_1 E_0 t\,(1+\bar{\alpha})\,\frac{t^2}{h^2} \tag{4}$$

The buckling coefficient C_1 was taken as 7.98; this is based upon tests of aluminum isogrid shells reported in Reference 5.

The CFACI ribs were idealized as orthotropic plate elements for the prediction of local crippling. The rib element support provided at the nodes was assumed to be equivalent to full clamping; this was because of the substantial buildup of material at the nodes and an effective increase in rib width that weaving or braiding create near the nodes. The rib-skin attachment was assumed to be equivalent to simple support. Thus, for an orthotropic plate clamped on two opposite edges and simply supported and free on the other two, the critical value of the stress resultant can be estimated from

$$N_{CR} = b^3 \left[\frac{4\pi^2 E_{11}}{12\, a^2 \left(1 - \nu_{12}^2 \frac{E_{22}}{E_{11}} \right)} + \frac{G_{12}}{d^2} \right] \qquad (5)$$

a is the rib length. E_{11}, E_{22}, G_{12} and ν_{12} are the usual elastic constants associated with the principal material directions; they were estimated from the micromechanical equations used in the McDonnell Douglas computer program ORACLES[6].

The cylinder design was conducted by parametric studies based upon Equations (1) and (4). Equation (5) was used to check trial configurations to ascertain if rib crippling is critical. (In the range of parameters studied, rib crippling did not influence the design.) The final design analysis phase for the shells consisted of a stiffened shell buckling analysis of general instability using a McDonnell Douglas computer program designated H485. This program is based upon the Flügge buckling equations, a smeared or averaged representation of the stiffeners, and the assumption of classical simply supported ends. This analysis refined the estimates obtained from Equation (1) to account for shell length and discrete wave number effects.

General instability of flat CFACI panels as wide columns was analyzed on an elementary basis. The following equation was utilized:

$$N_{CR} = \frac{\pi^2 E_o \bar{I}}{\lambda^2} \tag{6}$$

$\bar{I}$ is the effective transformed moment of inertia per unit width of panel for a composite cross section of ribs and skin; it is given by[2]

$$\bar{I} = \frac{t^3 \bar{\beta}^2}{12(1+\bar{\alpha})} \tag{7}$$

λ is the effective simply supported length of the column. Skin buckling and rib crippling for the panels were predicted from Equations (4) and (5) as in the case of the cylinders.

Cylindrical Shell Design

An extensive parametric design study was conducted for 20 inch diameter CFACI cylindrical shells. A 24 inch length was selected early in the study as it appeared a practical choice for future manufacture. The final selected design is illustrated in Figure 4. Predicted buckling loads and rib and skin stresses are summarized in Table 3.

Results of trade studies leading to the selected isogrid configuration are summarized in Figures 5-8. Skin buckling influences triangle height (h) and skin thickness (t). Rib depth (d) and thickness (b) are determined largely by general instability considerations. First, a skin thickness of 0.030 inch was selected based on manufacturing requirements to produce a hole-free braided skin. Next, the parameters h, d and b were investigated separately using a skin thickness of 0.030 as shown in Figures 5-7. For each parameter, a value was selected which produced an overall general instability buckling load less than 100,000 pounds and also less than either the skin buckling or skin strength envelope. Finally, the influence of variations in skin thickness

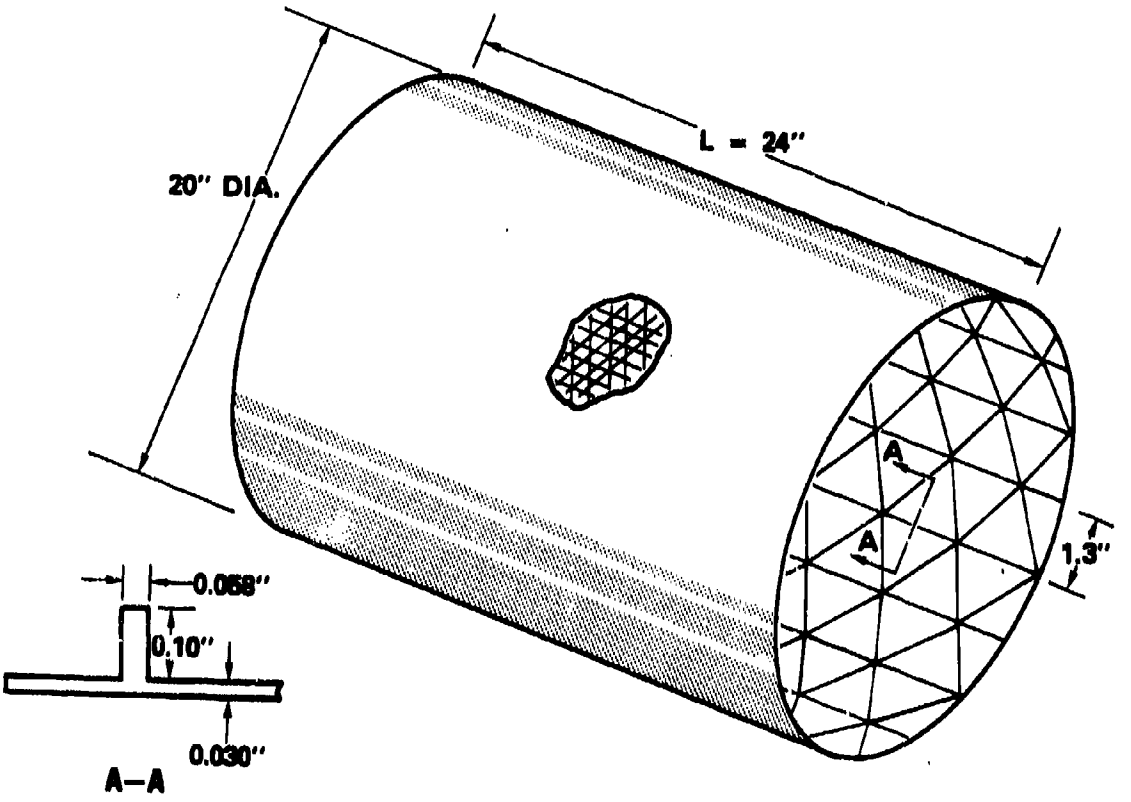

FIGURE 4. CYLINDRICAL SHELL DESIGN

GENERAL INSTABILITY

N_{CR} = 1360 lb./in. $\quad \sigma_{SKIN}$ = 33,200 PSI

P_{CR} = 85,500 lb. $\quad \sigma_{RIB}$ = 83,000 PSI

SKIN BUCKLING

N_{CR} = 1870 lb./in.

P_{CR} = 117,000 lb.

RIB CRIPPLING

N_{CR} = 16,792 lb./in.

P_{CR} = 1.055×10^6 lb.

TABLE 3. BUCKLING PREDICTIONS FOR THE CYLINDRICAL SHELL

PANEL BUCKLING

N_{CR} = 2130 lb./in. $\quad \sigma_{SKIN}$ = 33,200 PSI

P_{CR} = 22,200 lb. $\quad \sigma_{RIB}$ = 83,000 PSI

SKIN BUCKLING

N_{CR} = 2930 lb./in.

P_{CR} = 30,500 lb.

RIB CRIPPLING

N_{CR} = 6290 lb./in.

P_{CR} = 65,416 lb.

TABLE 4. BUCKLING PREDICTIONS FOR THE WIDE COLUMN

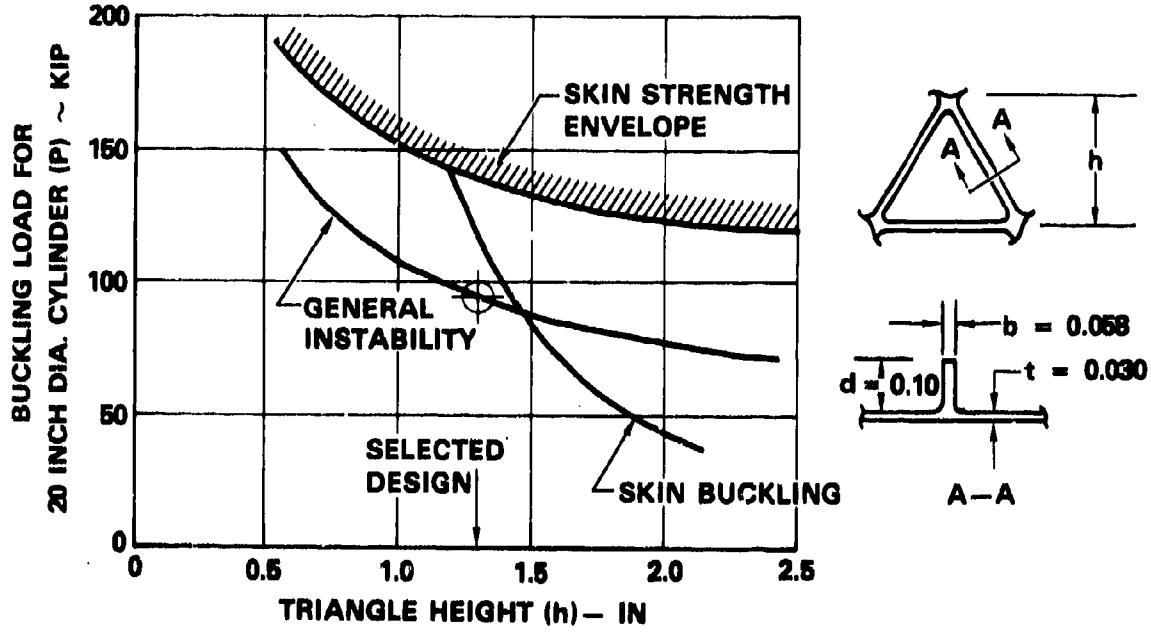

FIGURE 5. ISOGRID TRIANGLE HEIGHT DESIGN STUDY

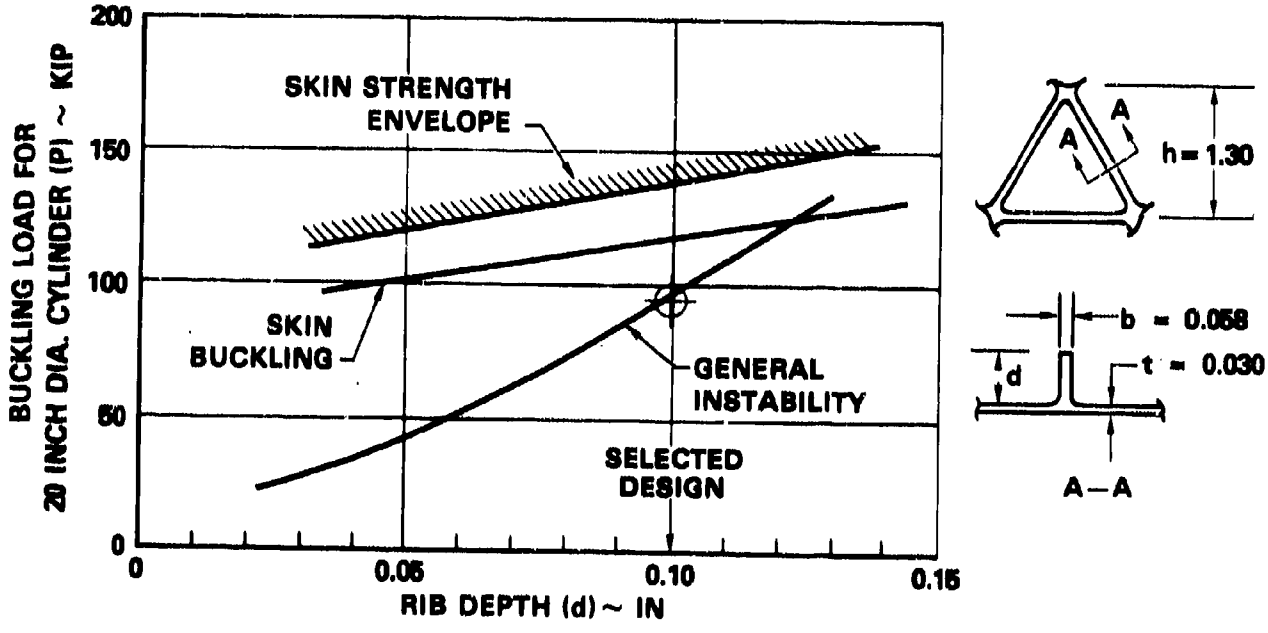

FIGURE 6. RIB DEPTH DESIGN STUDY

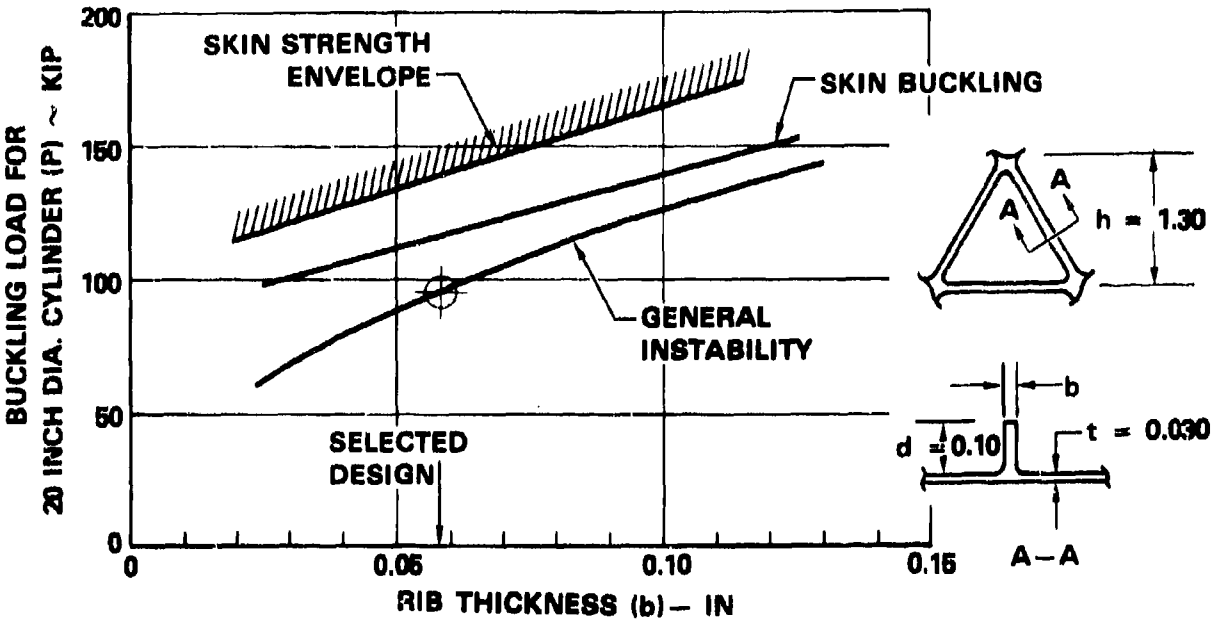

FIGURE 7. RIB THICKNESS DESIGN STUDY

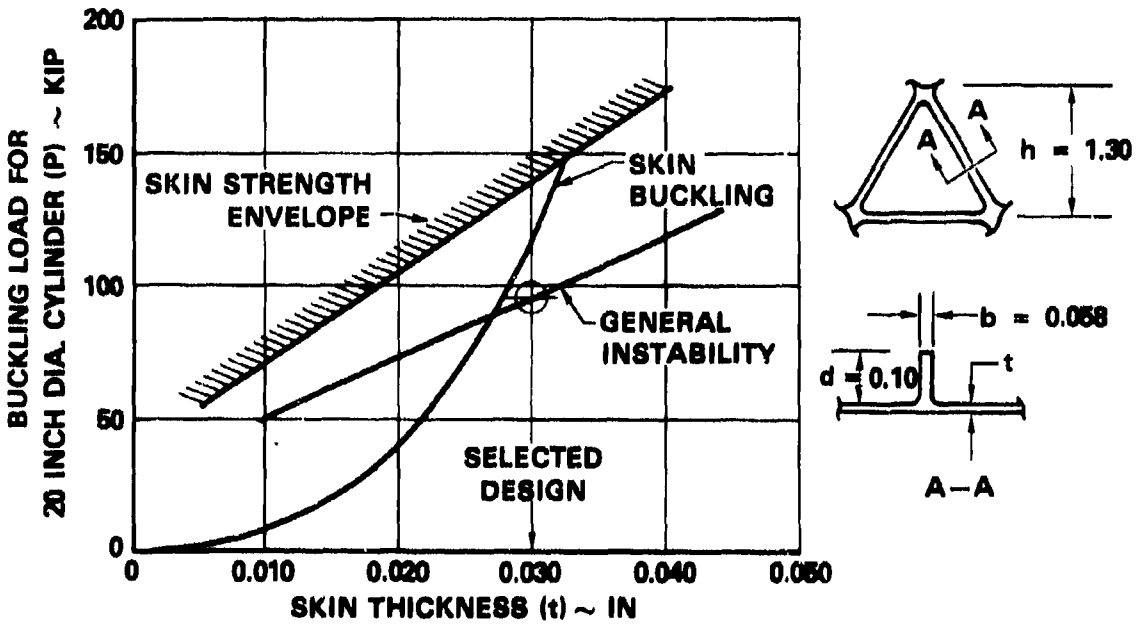

FIGURE 8. SKIN THICKNESS DESIGN STUDY

was also determined for the selected values of b, d and h as shown in Figure 8. None of the resulting rib geometries were rib-crippling critical.

As a final step, the H485 computer program was used to more accurately predict the general instability load and buckle wave shape. Results are summarized in Figure 9. The minimum buckling load is 2090 lb/in and the buckle wave pattern consists of two longitudinal half waves and six circumferential full waves. Applying a 65 percent knockdown factor[4] to the theoretical buckling load results in a predicted buckling load of 1360 lb/in. This corresponds to a total applied load of 85,500 pounds.

Note that the envelope of the six and seven circumferential wave curves in Figure 9 show an insensitivity to the number of longitudinal half waves for two or more half waves. This suggests that length and boundary restraint effects should be small for the selected design. This is desirable as the influence of these effects, although important, is not the objective of this research.

Wide Column Design

As mentioned earlier, in this first phase of the research, flat panels were to be built and tested as wide columns. A later phase was planned for actually building and testing cylindrical shells. Consequently, the maximum degree of applicability of the panel data to the shells was a primary objective. The cost of cylinders is much greater than that of panels, so it is prudent to reduce the risk associated with unanticipated modes of failure first with the less costly panel experiments.

A wide column design was selected having the same isogrid triangle geometry, stiffener and skin thickness and the same critical strain levels as the 20 inch diameter cylinder. Rib depth was increased to obtain a reasonable longitudinal buckle half wave length. The resulting design is shown in Figure 10.

A trade study which led to the selection of rib depth is summarized

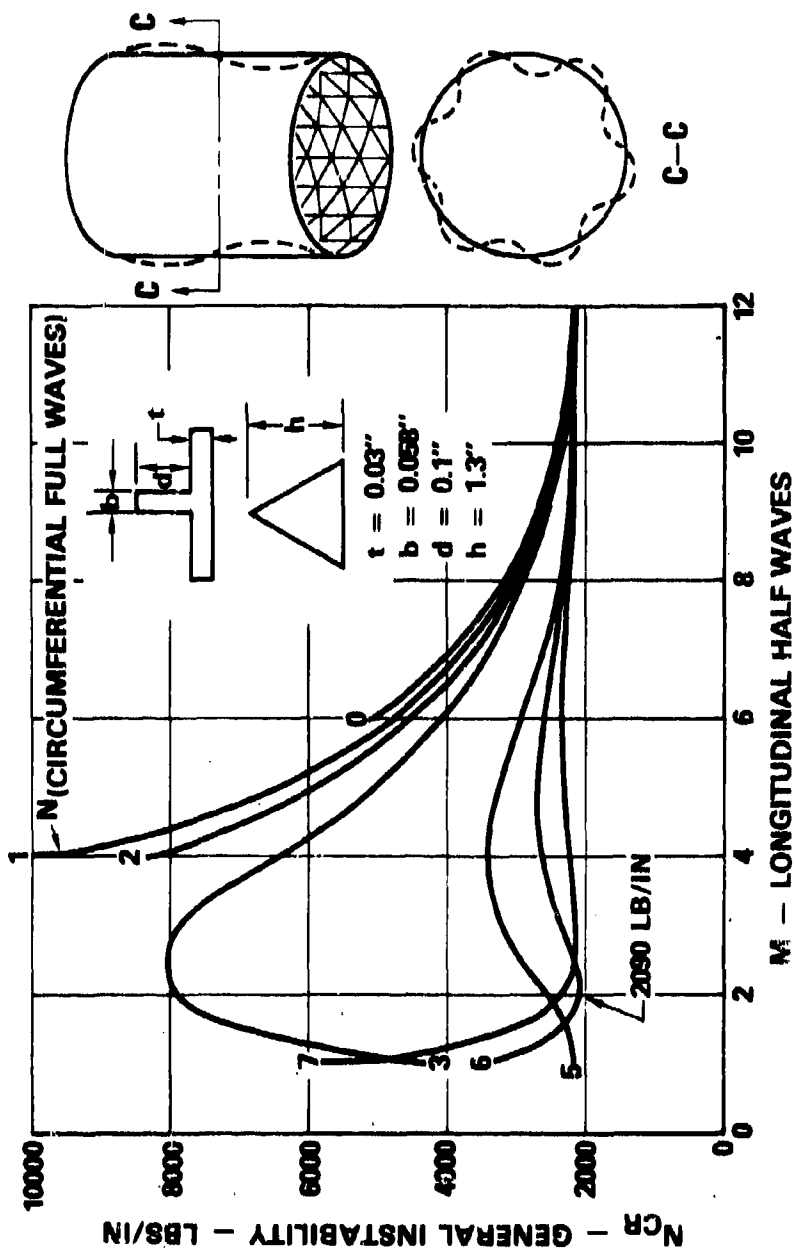

FIGURE 9. GENERAL INSTABILITY PREDICTIONS

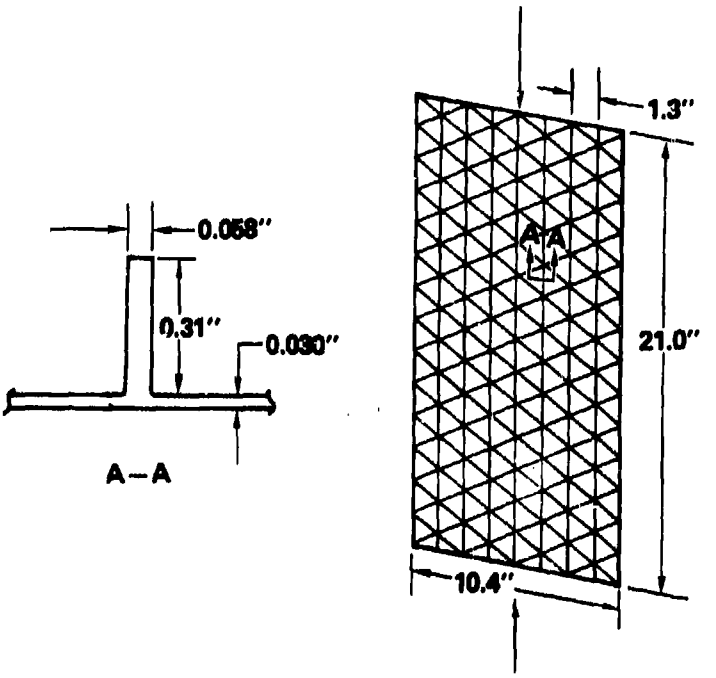

FIGURE 10. WIDE COLUMN DESIGN

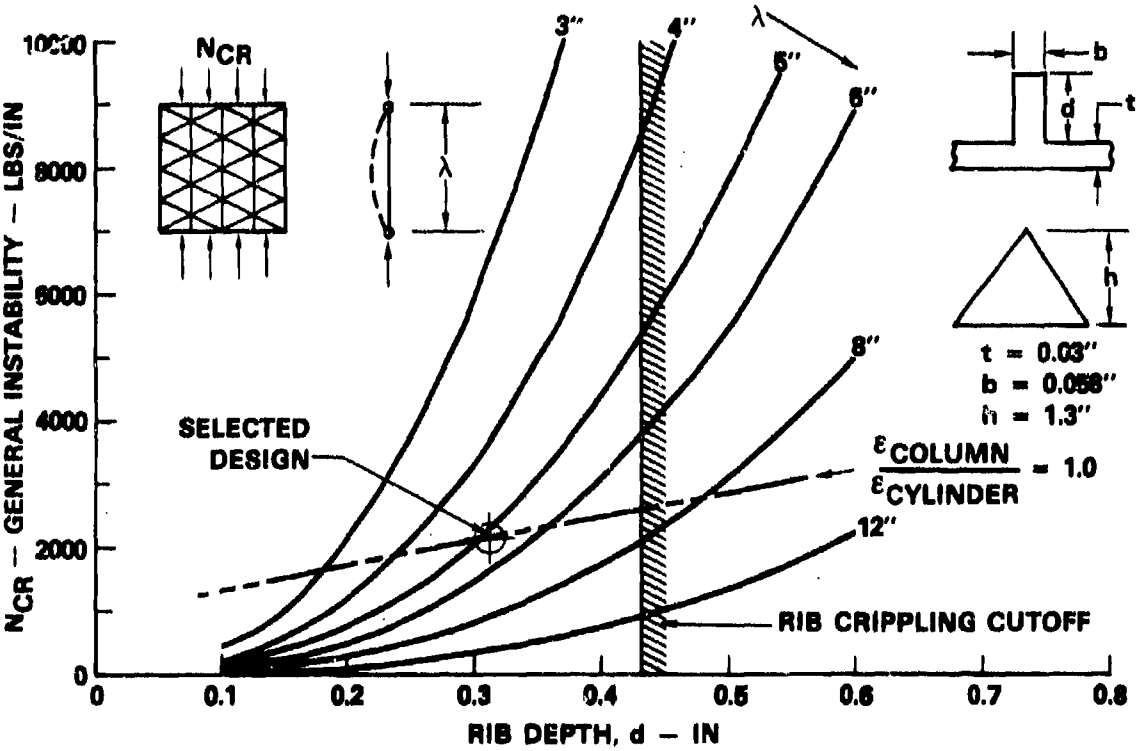

FIGURE 11. WIDE COLUMN GEOMETRY SELECTION

in Figure 11. General instability load is plotted versus rib depth (d) for various half wave lengths (λ). A half wave length of 5.25 inches and rib depth of 0.31 inch were selected which result in the same skin and rib strains (ϵ) at the time of general instability for the wide column as for the cylinder ($\epsilon_{column} / \epsilon_{cylinder} = 1.0$). The 5.25 inch buckle half wave length was to be achieved in test by properly restraining the panel. Predicted buckling loads are summarized in Table 4.

The buckle wave length of 5.25 inches is several times larger than the triangle height (h) of 1.30 inches. This was the chosen length to minimize interaction of the local buckling modes and general instability and to permit the smeared stiffener theory to be used with confidence.

MANUFACTURE OF FLAT PANELS

Introductory Remarks

A brief overview of the CFACI manufacturing process has been given in the introduction. A key element in this process is the design and manufacture of the tool for making the isogrid rib lattice. Consequently, this is described in the next section. It is followed by a description of the fabrication of the panels that have been tested as wide columns.

Tooling

The tooling was designed and fabricated to permit the skin and isogrid lattice to be joined by co-curing. The basic female tool serves both as a loom for guiding the dispensed prepreg yarn for reinforcing the ribs and as a mold for forming the ribs to their final dimensions from epoxy. It is made of one-piece construction from silicone rubber. The thermal expansion of the silicone rubber at the cure temperature of the epoxy resin is the means of applying pressure for compaction of the rib lattice. The effective rubber thickness adjacent to the prepreg yarn was controlled by calculated voids cast into the rubber so that the rib lattice system is exposed to a 50 psi cure pressure at the gel temperature (T_{gel}) of the matrix resin (approximately 280°F). This required the development of a method by which the silicone rubber voids could be configured to develop the correct bonding pressure at the proper temperature in the cure cycle without failing the tool at maximum temperature. The method used did not rigorously account, however, for the three-dimensional nature of the closure of the voids.

The stages of thermal expansion of the silicone rubber molding are illustrated in Figure 12 for a simplified, one-dimensional case. The rubber first freely expands across any open gap due to non-restricted linear thermal expansion (exaggerated) until it contacts the prepositioned prepreg yarn group at point (b). Compaction of the prepreg is then accomplished under increasing

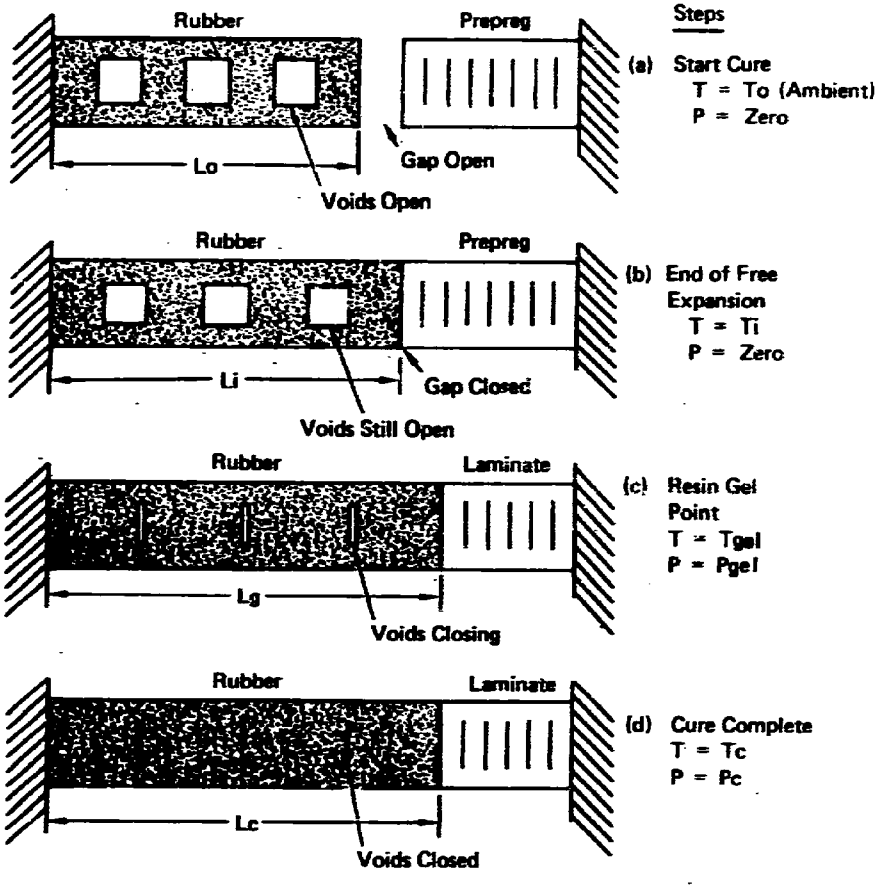

FIGURE 12. STAGES OF SILICONE RUBBER MOLDING EXPANSION

pressure with further increases in temperature until the resin gels at point (c). At the gel point, the laminate has been compacted to its final molded thickness under pressure P_{gel}. As the temperature is raised to the final cure temperature, pressure exerted by the rubber increases rapidly, but has little effect on the thickness or properties of the now-solid laminate. These stages of the process may also be presented as a pressure-temperature plot illustrated in Figure 13.

This one-dimensional model and approach were modified and improved to account for the three-dimensional expansion and associated compression of the silicone rubber cavities upon heating and pressure generation. First, data and the following equation were taken from Reference 7 to predict an effective modulus of the silicone rubber in terms of basic rubber physical properties and loading and shape parameters:

$$\frac{1}{E_{EFF}} = \frac{1}{E} \frac{1}{(1+2KS^2)} + \frac{1}{E_B} \qquad (8)$$

E_{EFF} is an effective modulus for the rubber in three-dimensional expansion, E is Youngs modulus and E_B is the bulk modulus. K is an empirical material factor, and S is a shape and loading factor.

Next, measured pressure test data from Reference 8 for silicone rubber blocks with cavities was compared to predictions using the above expression. Reasonable agreement was observed and further silicone rubber tooling sizing was based on the three-dimensional test data of Reference 8, supplemented by the above expression.

A full set of tooling was fabricated based on the pressure prediction techniques described above. It is shown in Figures 14 through 21. First, individual aluminum inserts were machined and attached to an aluminum base plate with pins. Framing dams and a plexiglass cover plate were then installed

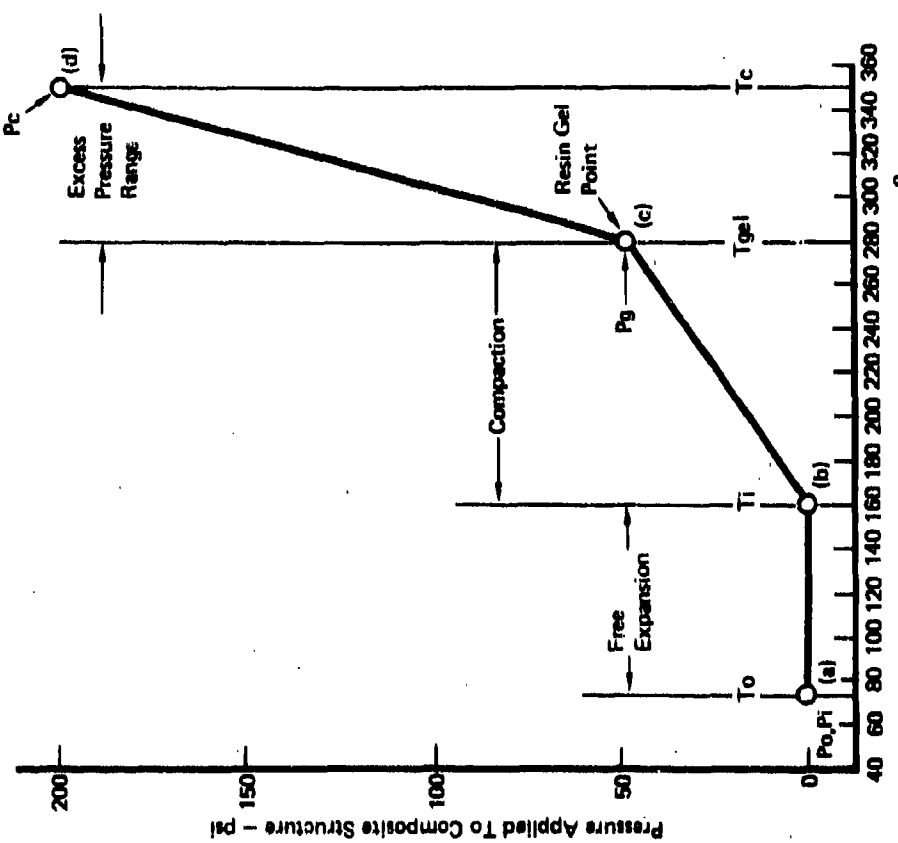

FIGURE 13. CONCEPTUAL PRESSURE – TEMPERATURE PLOT

which creates a closed mold (Figure 14). Into this mold an epoxy tooling compound is injected which, when cured, results in a dummy structure identical to the desired isogrid structure (Figure 15). The second major step consisted of transferring the hole patterns for both the pins which create the voids in the rubber and the pins at the nodal points to another aluminum base plate and machine drilling the holes. The final step consisted of reassembling the base plate containing void pins, nodal pins, dummy isogrid structure, dams and plexiglass cover plate; this creates a closed mold for the casting of the silicone rubber female isogrid molding (Figure 16). Figures 17 and 18 show the top and bottom of the female molding, respectively.

Once the female rubber molding was complete, it was attached to another aluminum base plate by means of nodal pins and plastic clusters. The cluster, Figure 19, is a plastic insert of a wheel configuration which provides additional yarn dispensing guidance at the nodal pins, yarn lay orientation, and resin/fiber content control. The completed tool is shown in Figure 20.

Fabrication

The fabrication process for the flat panels originally consisted of four major operations; weaving the isogrid ribs, braiding the skin mats on a round mandrel, laying up the skin and positioning the ribs and skin and co-curing them. However, after the initial panel was cured, the removal of the panel from the tooling proved difficult due to the large number of nodal pins over a relatively small panel area. The panel was removed only after considerable damage to the skin. Subsequently, the fabrication process was altered. The skin and ribs were cured separately and a secondary adhesive bond was then used to join the two.

The general weaving process for the flat isogrid ribs utilizes an automatic drafting machine modified to dispense prepreg yarn in a computer-controlled isogrid pattern (Figure 21). The head follows a pre-developed path throughout the isogrid pattern so that the fibers are nearly straight and the tensile strength of the fibers is not greatly impaired (Figure 22). After the required

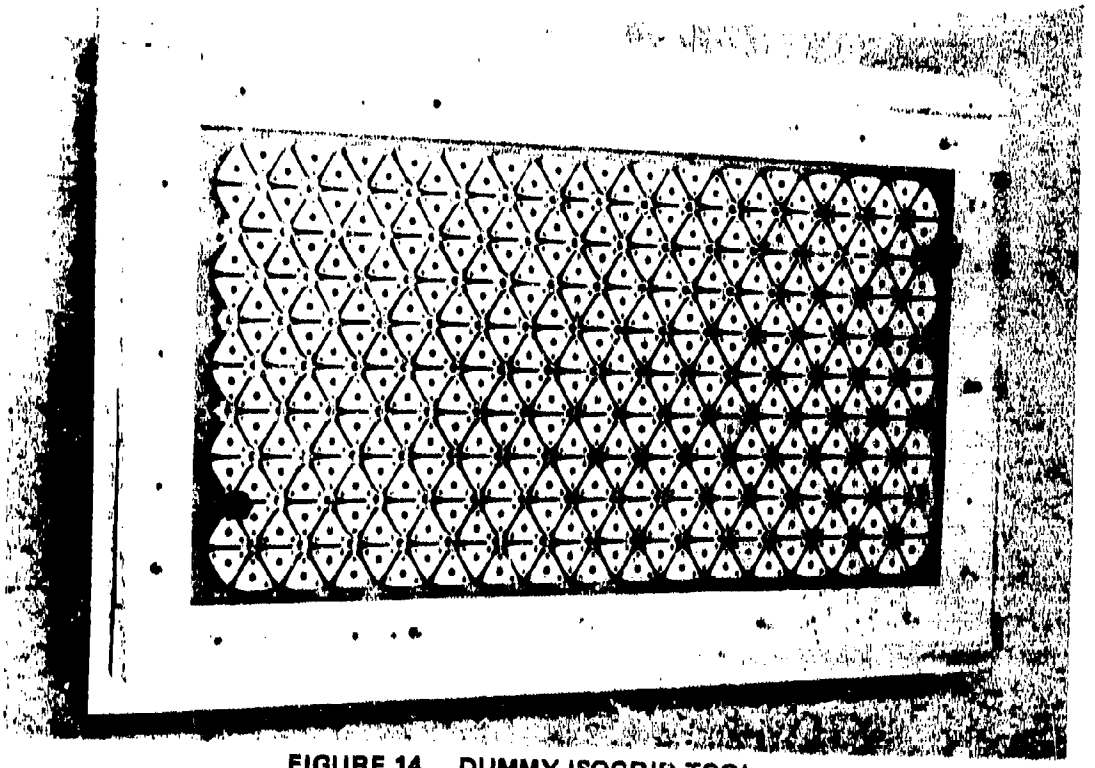

FIGURE 14. DUMMY ISOGRID TOOL

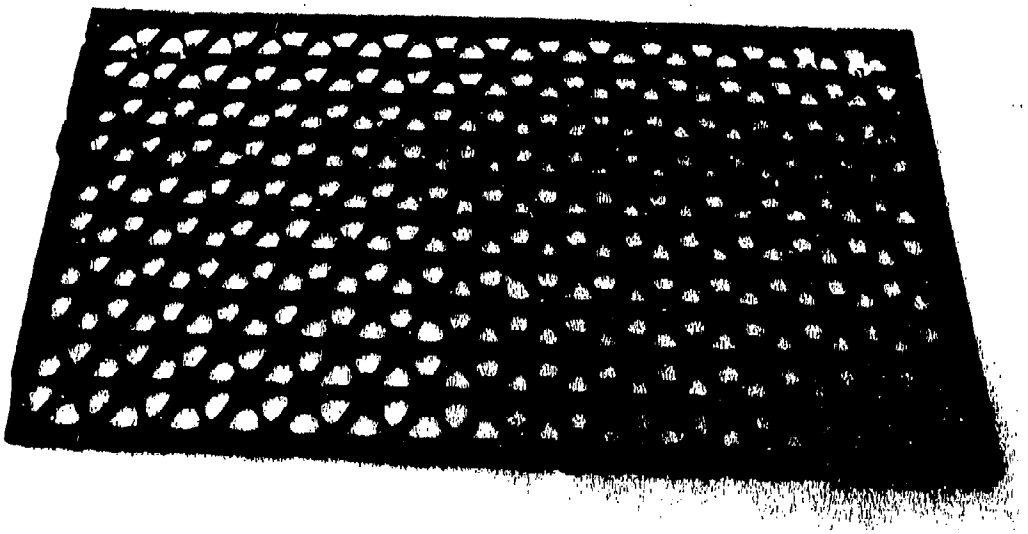

FIGURE 15. DUMMY ISOGRID

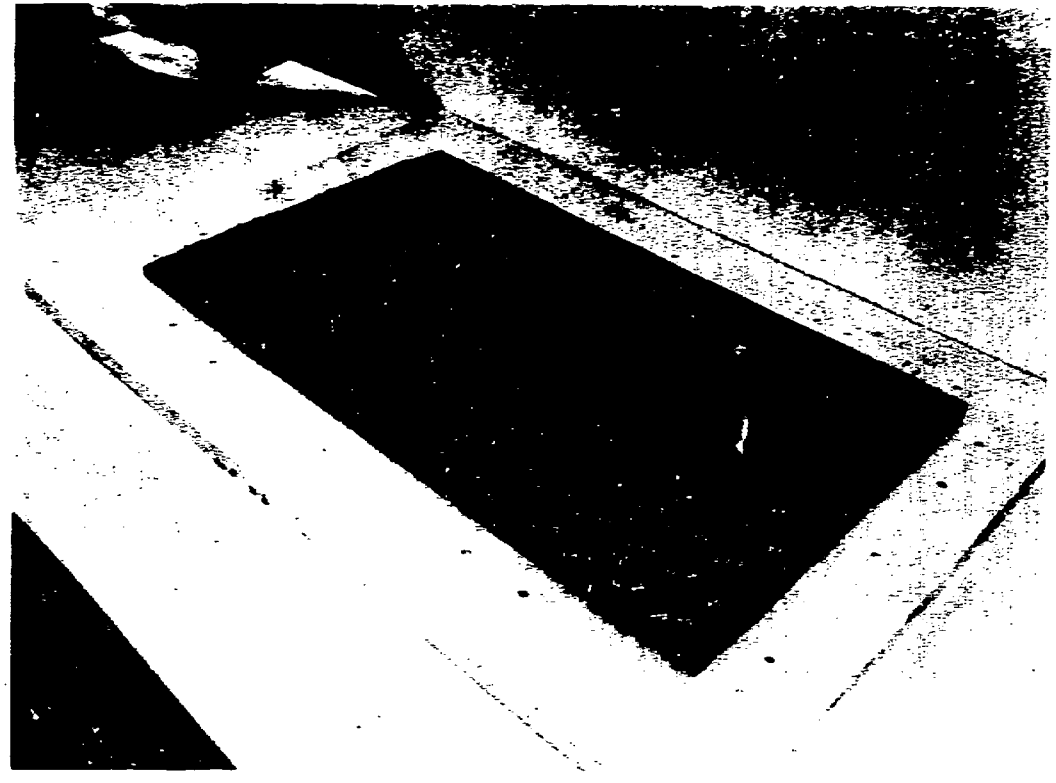

FIGURE 16. TOOL FOR CASTING FEMALE ISOGRID MOLD

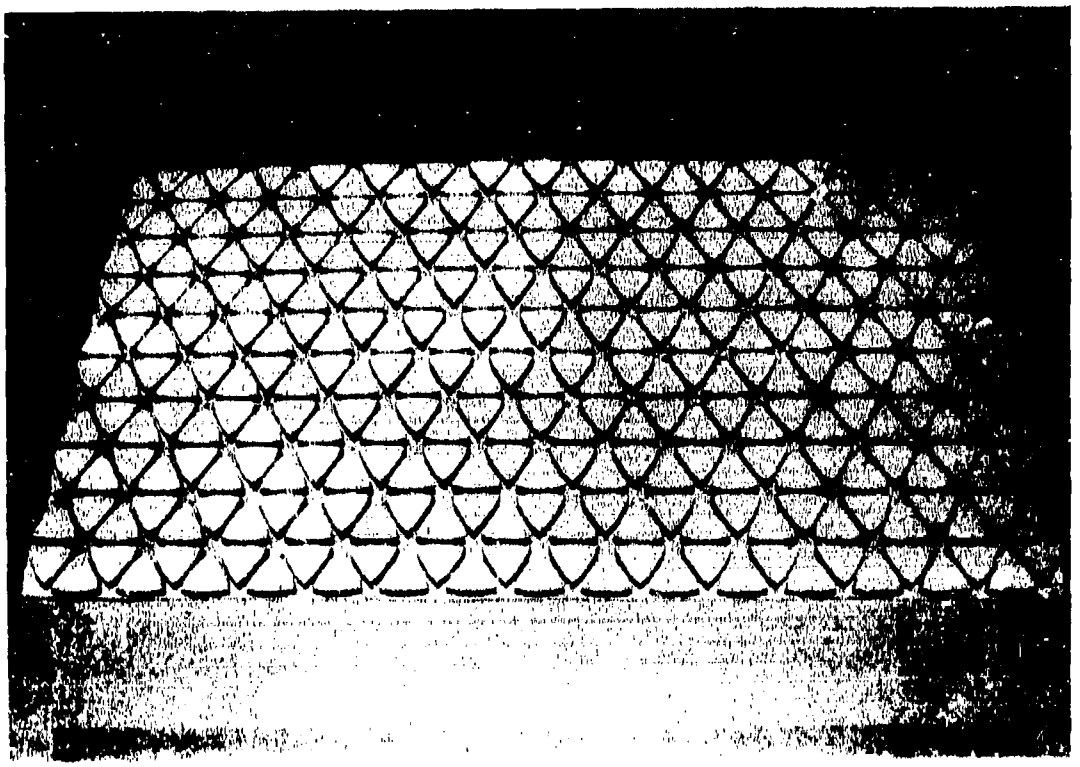

FIGURE 17. TOP VIEW OF FEMALE ISOGRID MOLD

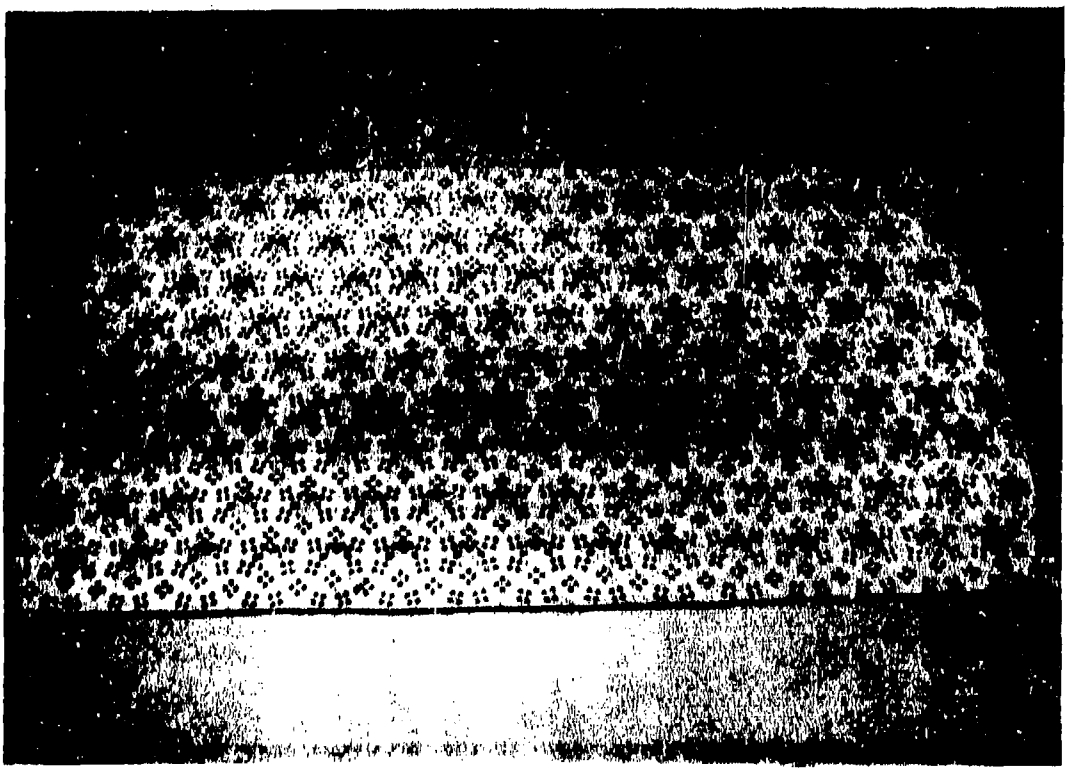

FIGURE 18. BOTTOM VIEW OF FEMALE ISOGRID MOLD

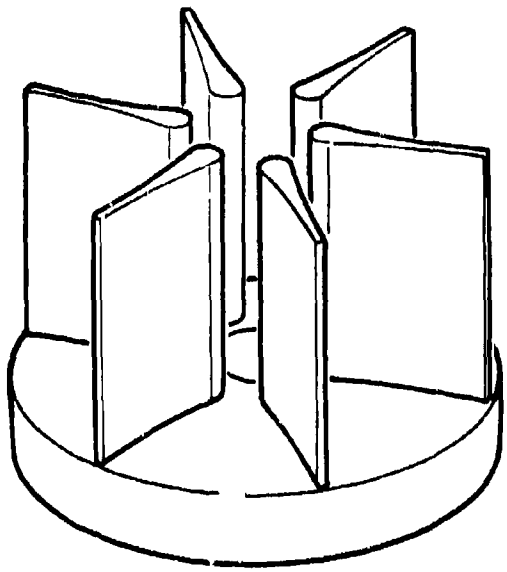

FIGURE 19. PLASTIC NODAL CLUSTER FOR CONTINUOUS FIBRE COMPOSITE TOOLING

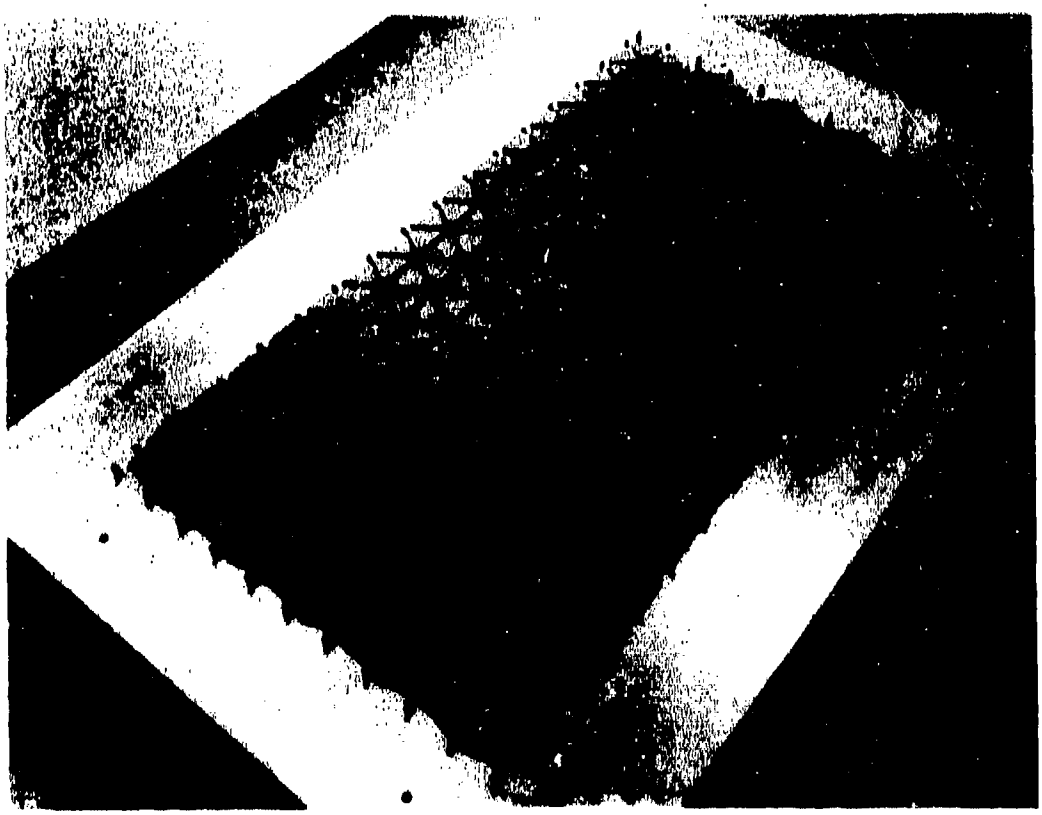

FIGURE 20. COMPLETE ISOGRID TOOL

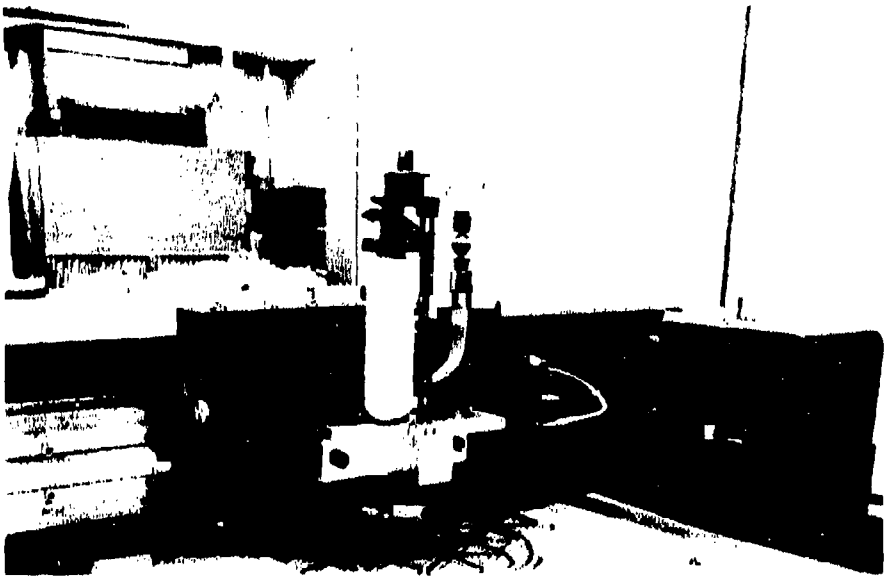

FIGURE 21. FLAT WEAVE PROCESS

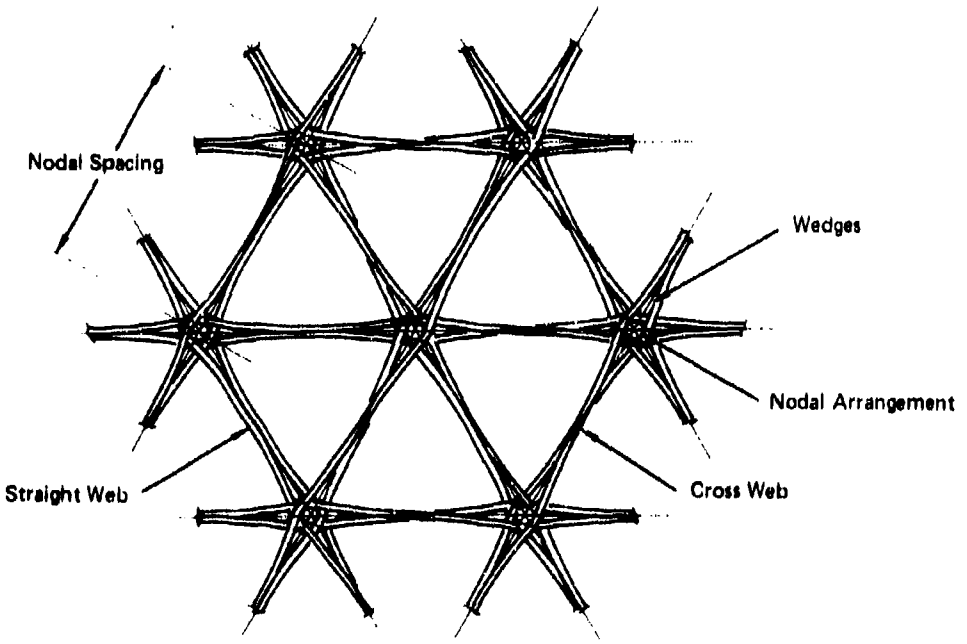

FIGURE 22. GENERAL CONCEPT CONTINUOUS FIBER COMPOSITE STRUCTURE

amount of yarn is dispensed, the structure is prepared for cure at 350°F for two hours. Side and top platen are set in place and the entire form is held together with a bolted I-beam support structure.

Prepreg mats were braided from 1/4 inch wide tape in a $[0,\pm 60]$ configuration A circular mandrel was used for the braiding (Figure 23); the mats resulted from removing the continuous braid by cutting and unrolling it. The quasi-isotropic skins were formed by stacking four mat plies (Figure 24) and curing by conventional techniques.

The isogrid rib lattice was secured to the skin by a secondary adhesive bond. A film adhesive, American Cyanamid FM-123-2, was used according to MAC process standard 11308. The end zones of the panels were then potted to facilitate the introduction of load in testing. Figures 25 and 26 show a completed panel.

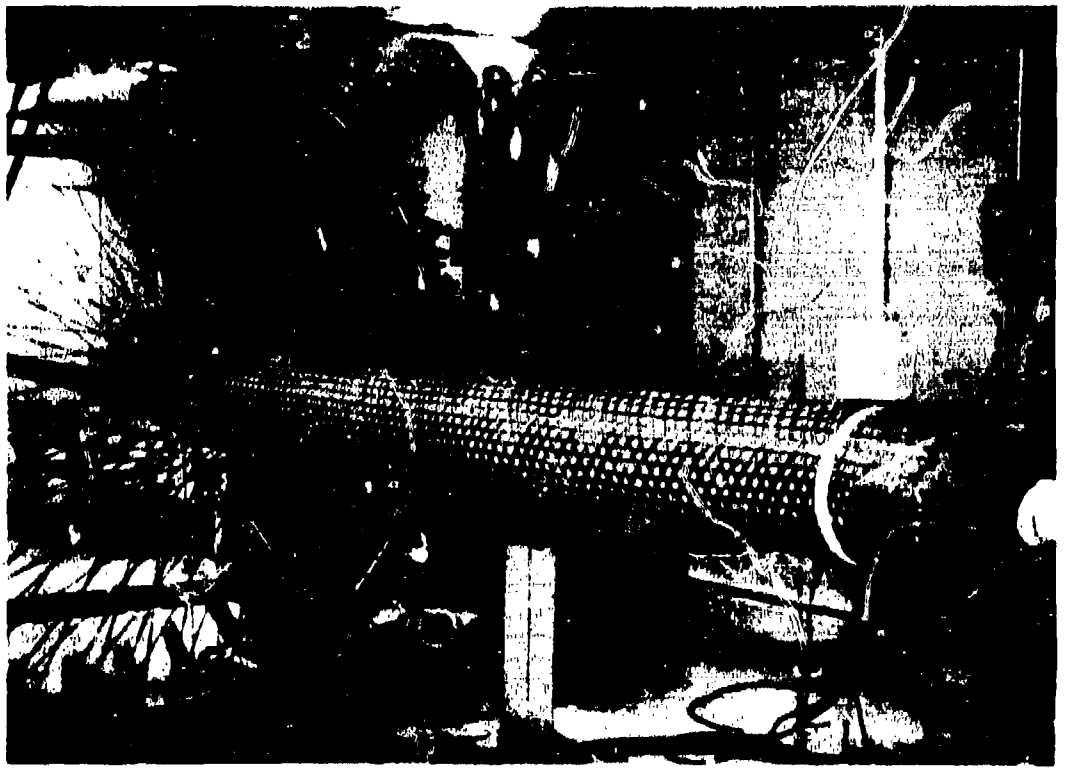

FIGURE 23. BRAIDING SKIN

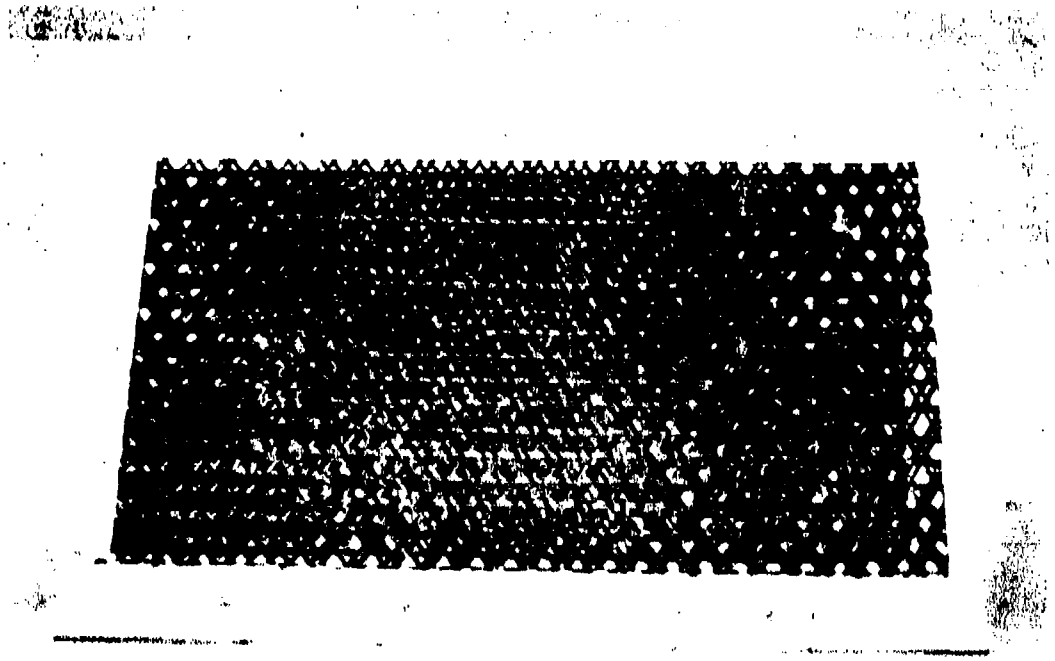

FIGURE 24. LAY–UP OF SKIN PRIOR TO CURE

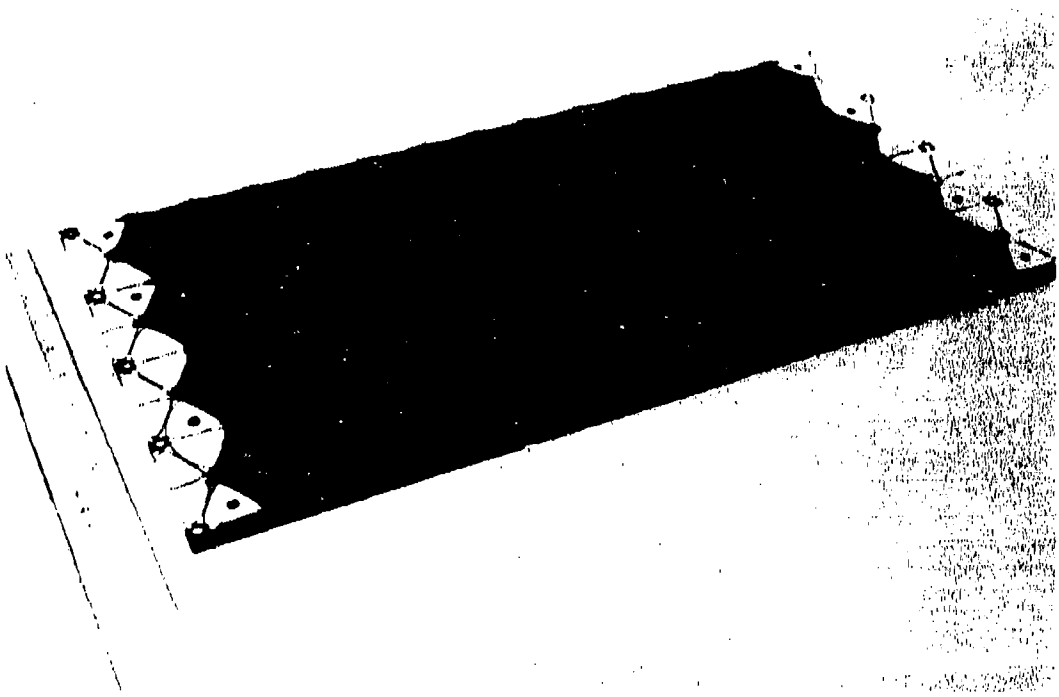

FIGURE 25. ISOGRID PANEL – RIB SIDE

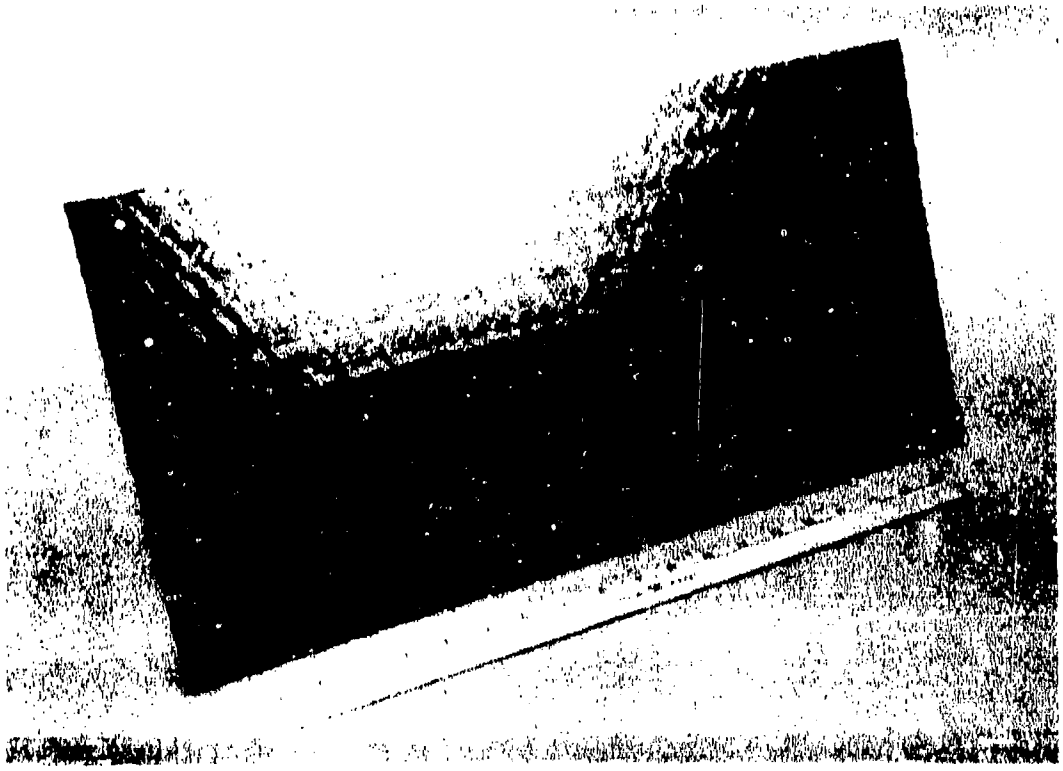

FIGURE 26. ISOGRID PANEL – SKIN SIDE

EXPERIMENTAL PROGRAM

Overview

The 21.00 inch panel length, together with an effective column length of 5.25 inches, was selected so that the desired critical buckling strain could be achieved in two ways. First, this effective column length corresponds to the third buckling mode of the panel if both ends are fully clamped. An extrinsic stiffening concept was developed to suppress buckling in the lower modes in the hope that buckling in the third mode could be determined experimentally. Second, in the event that third mode buckling proved too difficult to achieve within the time limitations imposed by the contract, the panels could be cut in half and tested fully clamped. The first buckling mode of a 10.50 inch fully clamped panel corresponds also to a 5.25 inch effective column length. As it turned out, only partial success was achieved with the extrinsic stiffening frame employed, so the second option was exercised.

The panels were tested under progressively increasing loads with buckling events nondestructively estimated by a stiffness plotting technique. The original program called for the determination of the first, second and third buckling loads. This was modified, as indicated earlier, by discontinuing the search for third modes and determining the first modes of fully clamped panels of half the original length. Any unforseen influences associated with boundary restraint effects were sought by determining multiple buckling loads for the panels.

In addition to the buckling tests mentioned above, three panels were trimmed to smaller widths and compression tested in order to explore the applicability of smeared stiffener theory. Also, overall extensional stiffness was monitored during compressive loading and three-point bending tests were conducted. These latter results will be presented with element tests data in another report.

CFACI Panel Specimens

The initial panel that was manufactured with co-cured ribs and skin was scrapped as extensive damage occurred while removing it from the tooling. Three panels were then manufactured with ribs and skin attached by secondary bonding using a film adhesive. These were designated 1, 2 and 3 corresponding to the order in which they were produced and delivered to GIT.

A change in tooling was made for the manufacture of panel 3. Panels 1 and 2 were produced with the plastic clusters (Figure 19) imbedded in the rib pattern. Since this practice increases the weight of the panel measurably, panel 3 was made in another way. In place of the clusters, silicone rubber wedges arrayed in a similar pattern were used for this panel. These wedges could be removed in the same manner as the basic female tool after curing of the rib lattice. Also, the thermal expansion of the wedges produced increased compaction in the vicinity of the nodes.

A sample fiber volume fraction measurement was made of scrap trimmed from panel 1; a 61 percent fiber content by volume was found.

A survey of geometric dimensions was conducted for each of the three panels. Mean values of dimensions determined from ten distinct measurements are given in Table 5. Notice that skin thickness and rib depth are reasonably consistent from panel to panel. Rib width, however, varied substantially; this variation has been tentatively attributed to silicone rubber control of pressure during fabrication. This characteristic is being investigated further at MDAC-E to permit more uniform part manufacture in the future. The ribs have essentially the same number of fibers in all cases; it is the resin content and geometrical shape that differ among panels. It is not clear whether the tooling change for panel 3 markedly influences its rib width.

Nondestructive Estimation of Buckling Loads

There are several reliable nondestructive buckling load estimation tech-

PANEL	$\bar{t}$, IN.	$\bar{b}$, IN.	$\bar{d}$, IN.
1	0.0548	0.0828	0.311
2	0.0568	0.0670	0.309
3	0.0556	0.0566	0.291

TABLE 5. MEAN GEOMETRIC CHARACTERISTICS OF PANEL SPECIMENS

MODE NO.	P_{cr}, LBS. (ANALYSIS)	P_{cr}, LBS. (EXPERIMENT) PANEL NO.		
		1	2	3
1	5,550	7,200	6,200	4,600
2	11,336	14,000	12,100	9,125

TABLE 6. BUCKLING RESULTS FOR LARGE ISOGRID WIDE COLUMNS

niques that can be used for structural systems that are not imperfection sensitive. A thorough survey is given in Reference 9. All available methods are founded upon means for detecting reductions in stiffness under increasing, but subcritical, values of destabilizing load. The particular stiffness plotting technique that has been used is attributed to Donnell[9]; it apparently was rediscovered independently by Jones and Greene[10].

The basis for the method is the fact that geometric imperfections are always present to some degree in real structures and that, as a result, a response in the buckling mode can be detected at subcritical values of load. This situation applies only to structures which would buckle by bifurcation if perfect. The lateral (flexural) deflection W associated with response in the buckling mode is assumed to obey an equation of the form

$$W = \frac{W_o}{\frac{P_{CR}}{P} - 1} \tag{9}$$

W_o is the value of deflection attributed to geometric imperfection, P is the destabilizing load and P_{CR} is the classical buckling load of the "perfect" structure. Consider load-deflection pairs (P, W) above initial values (P_1, W_1) that obey Equation (9). It is easily shown that the following equation is a consequence of (9):

$$\frac{(P-P_1)}{(W-W_1)} = (P_{CR} - P)\frac{\left(1 - \frac{P_1}{P_{CR}}\right)}{W_o} \tag{10}$$

The above equation has a simple physical interpretation. The ratio on the left hand side of the equation is an incremental measure of flexural stiffness. From the right hand side, it is found to vary linearly with load and to vanish at $P = P_{CR}$. Thus, in practice, the incremental stiffness is plotted for subcritical values of load. A straight line should be obtained

which can be extrapolated to zero stiffness. The load corresponding to the zero stiffness intercept is the buckling load according to classical theory. The resulting linear plots are referred to as modified Donnell plots or stiffness plots.

An extensive discussion of the use of stiffness plots and their interpretation if the data reflects nonlinearity is given in Reference 10. A typical plot is shown in Figure 27; it corresponds to first mode buckling of panel 1.

Experimental Technique

Successful compressive testing of the CFACI panels as wide columns required adequate and repeatable simulation of fully clamped boundary conditions and suitable instrumentation to monitor transverse displacement. In addition, a fixture was required for extrinsic stiffening to constrain the panel appropriately for obtaining higher buckling modes. The clamped boundary conditions were obtained by using a set of 1.50 inch angles bolted through the potted ends of the panel. The test setup used to produce the first (lowest) buckling mode appears in Figure 28; the end restraint configuration is evident in this figure.

Lateral deflections of the panels were measured with linear variable differential transformer (LVDT) displacement transducers. Normally the deflections at the center and quarter span points were monitored during compressive loading. This array of transducers appears also in Figure 28. The panel response could easily be decomposed into symmetric and antisymmetric contributions with respect to the panel center span with displacement data at these points.

The first three buckling modes of a fully clamped wide column are pictured in Figure 29. In order to produce the second mode, some means is required to enforce a node line at the column center (semi-span). If the third mode is desired, a response that is symmetric about the center node line is required

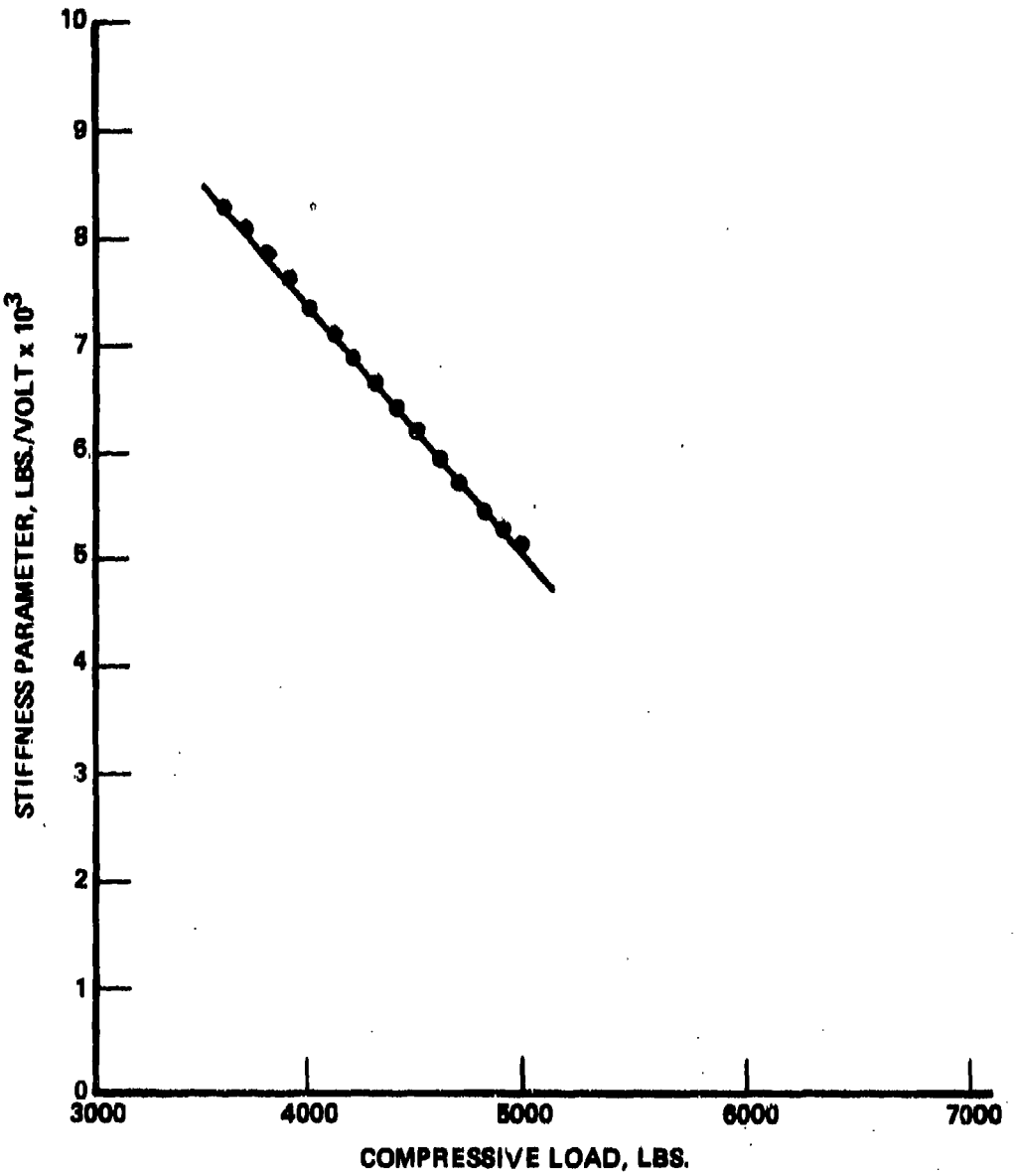

FIGURE 27. STIFFNESS PLOT FOR FIRST MODE OF PANEL 1.

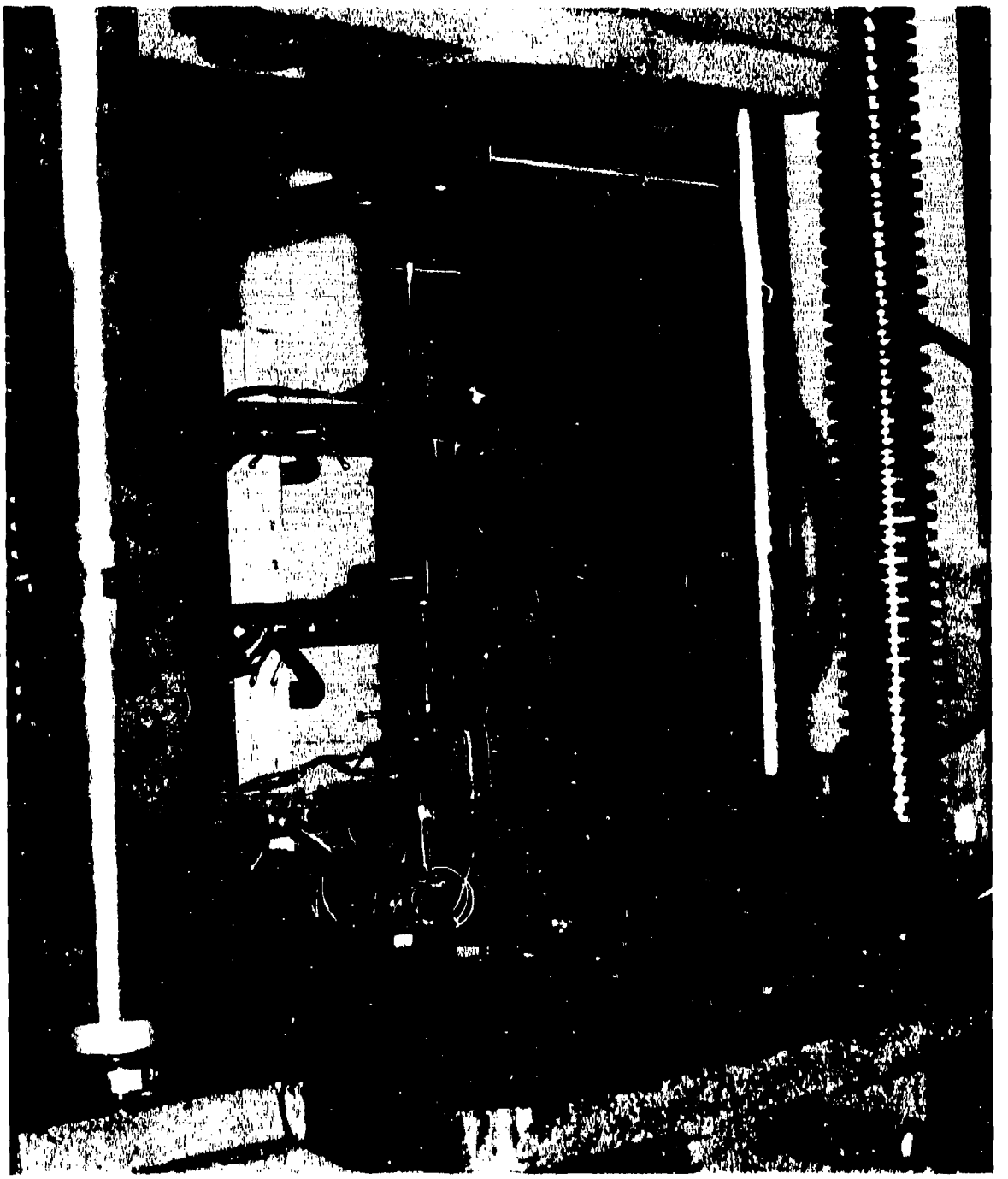

FIGURE 28. EXPERIMENTAL SETUP FOR FIRST BUCKLING MODE

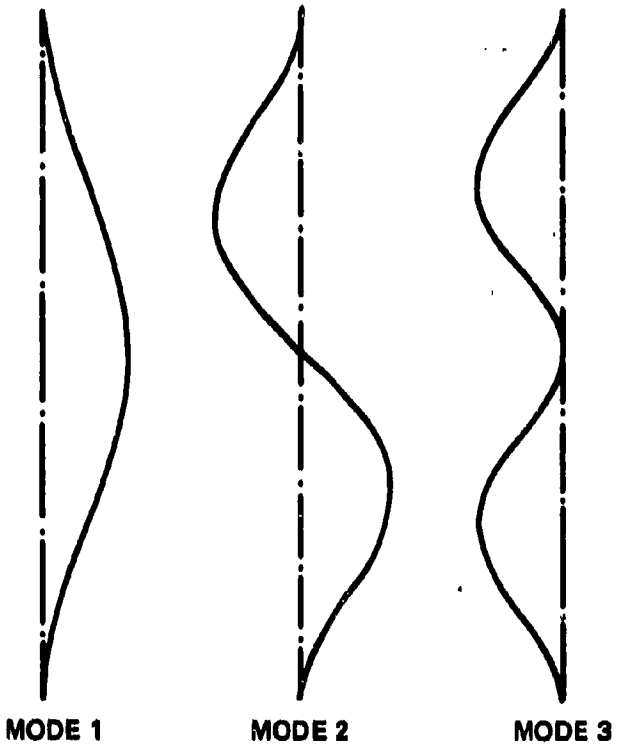

FIGURE 29. MODE SHAPES OF A WIDE COLUMN

in addition. A fixture was designed and fabricated to provide extrinsic stiffening in order to simulate these modes. The fixture and setup corresponding to the second buckling mode are shown in Figure 30. A single pair of supports (one on either side of the panel) is positioned at semi-span and retained by a frame mounted to the bed of the test machine. Although it is not apparent in Figure 30, three lateral displacements are measured, the center one associated with frame motion. For the determination of the second buckling load from a stiffness plot, the antisymmetric component of the column deflection (the difference of the quarter span displacements) serves as the generalized displacement.

The fixture and setup corresponding to the third buckling mode are shown in Figure 31. The optimum means of producing the third mode is to enforce a zero slope at the center span of the panel. Consequently, three closely spaced supports are utilized in the central region, the outer two of which are placed on one side of the panel only. In addition, two one-sided supports were added at the quarter span locations. The sole purpose of the one-sided supports is to enforce a symmetric mode of panel deflection.

Both configurations proved successful in obtaining the second and third modes of a 6061-T6 aluminum panel in pilot tests. Unfortunately, difficulties developed in attempts to determine the third mode of isogrid panels. Displacement data indicated that the center node line was not being maintained. Rather than redesign and stiffen the frame, only the second mode configuration was utilized. As indicated in the overview, the panels were cut into smaller panels and tested fully clamped.

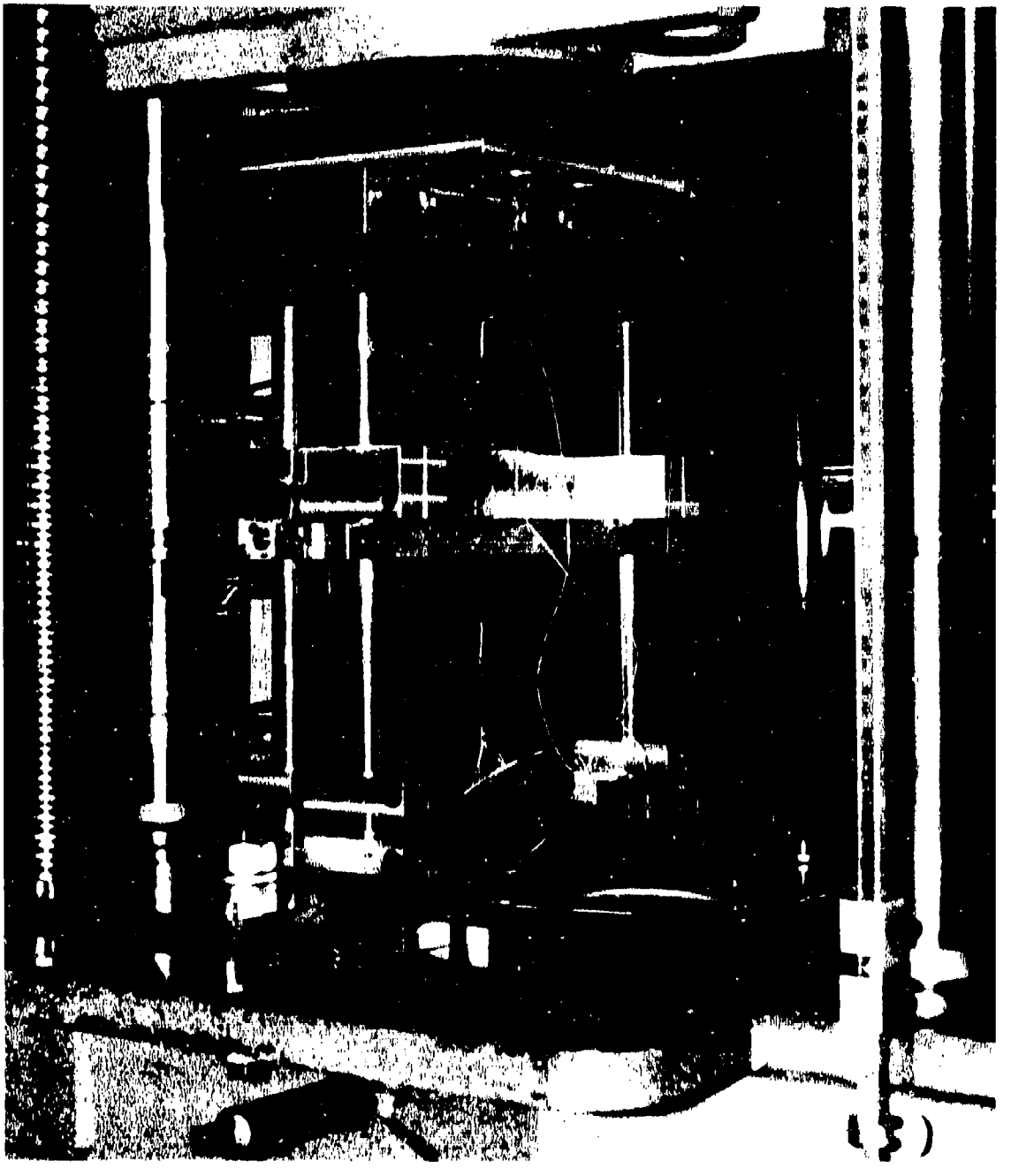

FIGURE 30. EXPERIMENTAL SETUP FOR SECOND BUCKLING MODE

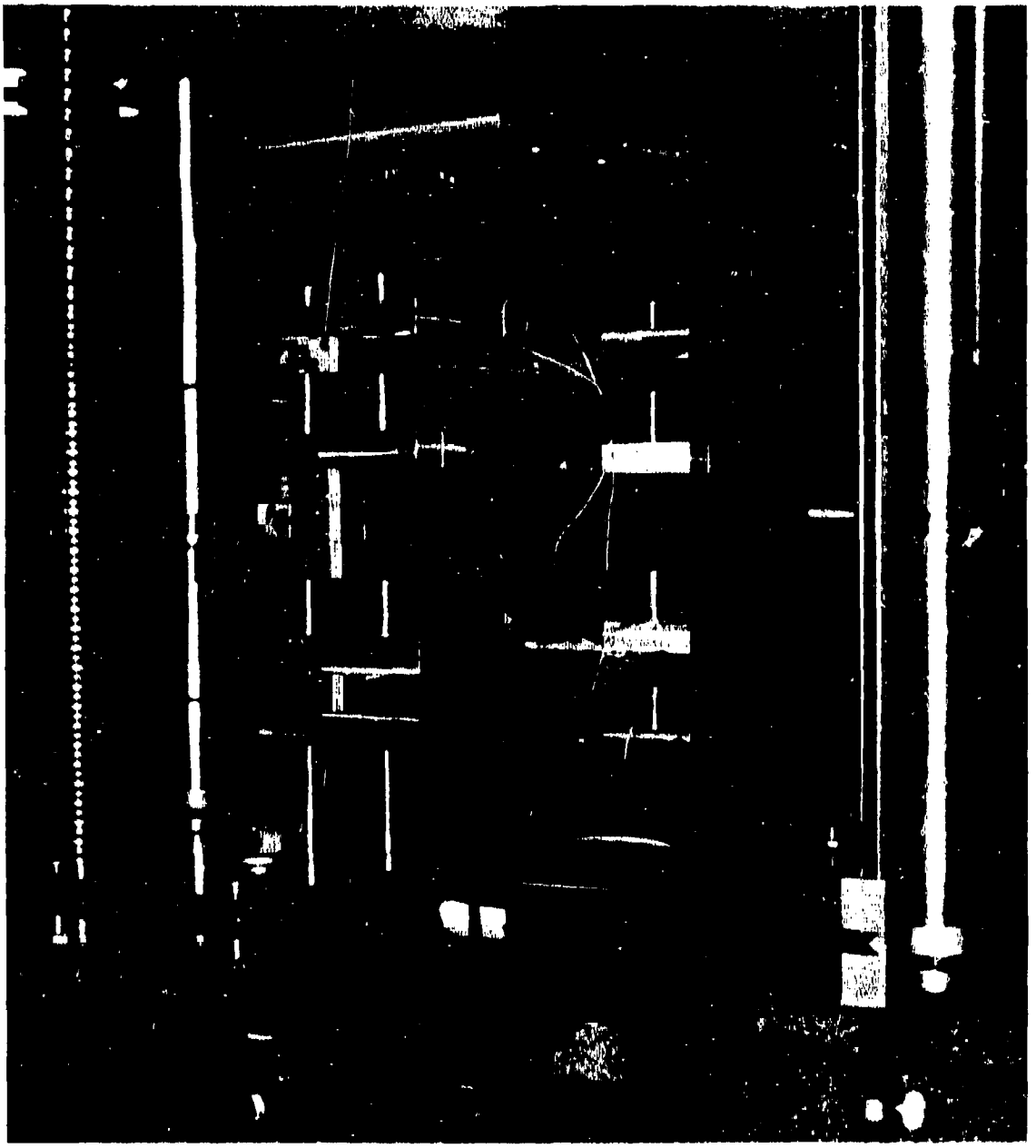

FIGURE 31. EXPERIMENTAL SETUP FOR THIRD BUCKLING MODE

RESULTS AND DISCUSSION

Large Panel Buckling Experiments

The results of buckling experiments conducted on the whole 21.00 inch long panels are summarized in Table 6. All critical load estimates were determined from stiffness plots and are believed to be accurate to within 100 pounds. An actual buckling event corresponding to the first mode of panel 3 occurred accidently; buckling at the relatively low load was not expected after the first two panels buckled at loads that exceeded design predictions. The actual buckling load and the one predicted by a stiffness plot of the data agree exactly in this instance, which was gratifying.

The entries in Table 6 (and Table 7) correspond to "best" estimates obtained after several repeated loading runs. "Best" implies (nearly) repeatable buckling load estimates and linear stiffness plots obtained at loads within 25 percent of the estimated buckling loads.

There is a wide variation in buckling loads among the panels. This issue will be discussed thoroughly subsequently. It is clear, however, that all the results are near enough to the design analysis prediction to suggest that the design approach is sound and that the panels generally behaved as anticipated.

Experimental determination of the first two buckling loads provides a means of assessing boundary restraint in an indirect way. Let $P_{CR\ i,j}$ denote the i-th (1st or 2nd) buckling load of panel j (1,2 or 3). From the results in Table 6

$$\begin{aligned} P_{CR2,1}/P_{CR1,1} &= 1.94 \\ P_{CR2,2}/P_{CR1,2} &= 1.95 \\ P_{CR2,3}/P_{CR1,3} &= 1.98 \end{aligned} \qquad (11)$$

The closeness of the above load ratios indicates that the test setup provided rather consistent boundary restraint. Furthermore, the theoretical value of the load ratio is 2.04 for fully clamped ends. A good approximation to ideal clamping was achieved, therefore.

Small Panel Buckling Experiments

Originally, the reason for desiring to determine the third buckling mode of the long panels was to minimize the influence of boundary restraint effects. There proved to be difficulties in doing this experimentally. However, the indirect assessment of boundary restraint provided by the two lowest buckling loads described above reduced the uncertainty regarding boundary restraint for this type of structure. Consequently, the decision to cut the large panels into smaller ones for first mode buckling tests did not interfere, but, in fact, enhanced the program. A much larger data base has been established.

The 21.00 inch long panels were each cut into four smaller panels. The small panels are nominally 10.50 inches long and 4.25 inches wide. The width was selected so that a center beam specimen containing a lengthwise rib was obtained from each large panel for subsequent element tests. The small panels are designated i-j, where i denotes the i-th large parent panel and j identifies the j-th small panel within the set of four.

Buckling test results for the small panels appear in Table 7. Also, mean values calculated from this data that correspond to each large parent panel are given. As for the parent panels, the data reflect a wide variation in buckling loads.

Nondestructive buckling load estimates for panels 1-4 and 3-3 were not determined. Panel 1-4 exhibited perplexing behavior. The central lateral deflection first increased in one direction and later, at higher load values, began to decrease indicating a tendency to buckle in the opposite direction. Because an element test program is to follow, a destructive buckling test

Panel	P_{cr}, lbs.	Panel	P_{cr}, lbs.	Panel	P_{cr}, lbs.
1–1	11,500	2–1	8,250	3–1	6500[1]
1–2	8,849	2–2	6,652	3–2	6619
1–3	9,500[1]	2–3	9,714	3–3	–[3]
1–4	8,384	2–4	–[2]	3–4	6182
$\bar{P}_{cr1}$ = 9,558		$\bar{P}_{cr2}$ = 8,205		$\bar{P}_{cr3}$ = 6,433	

NOTES: 1. Skin disbonded.

2. Erratic, unexplained behavior.

3. Excessive acoustic emission. Test aborted.

TABLE 7. BUCKLING RESULTS FOR SMALL ISOGRID WIDE COLUMNS

PANEL	N_{cr}, LB./IN. (UNTRIMMED)	N_{cr}, LB./IN. (TRIMMED)
1–1	2706	2356
2–3	2270	2145
3–2	1552	1541

TABLE 8. BUCKLING DATA FOR TRIMMED AND UNTRIMMED SMALL PANELS

was not performed. It is likely that a peculiar initial imperfection pattern is responsible for the failure to obtain an adequate stiffness plot for this panel.

Acoustic emission equipment was used to monitor panel response in a number of the compressive tests on the small panels. By this means, it was hoped that any unforseen failure modes could be detected prior to total failure and permit the test to be stopped. Skin-rib lattice disbonding occurred on panels 1-3 and 3-1 as acoustic emission was not used in these cases. (The data provided good stiffness plots for buckling load prediction in spite of the premature disbonding failures for these two panels, however.) Testing of panel 3-3 was discontinued because of excessive acoustic emission. Extensive damage of this panel was avoided so that a further investigation could be conducted at a later time.

Discussion

There are three important issues that are raised by the data presented in Tables 6 and 7. They are

(1) a rational, convincing explanation of the scatter in the data;

(2) the relationship between large and small panel buckling data;

(3) the relationship of the experimental data to theory.

All of the above are interrelated, so this separation is for convenience and, to some extent, is a matter of taste.

Issues (1) and (2) are best discussed together. Let $(\bar{P}_{CR1})$ denote the mean of the fundamental buckling loads for the three large panels given in Table 6; it is 6000 pounds. Note the following load ratios:

$$\left.P_{CR1,1}\right/(\bar{P}_{CR1}) = 1.200$$

$$\left.P_{CR1,2}\right/(\bar{P}_{CR1}) = 1.033 \qquad (12)$$

$$\left.P_{CR1,3}\right/(\bar{P}_{CR1}) = 0.767$$

Let $\bar{\bar{P}}_{CR1}$ denote the mean of the three mean values of critical loads ($\bar{P}_{CR1}$, $\bar{P}_{CR2}$, $\bar{P}_{CR3}$) given in Table 7 for the small panels; it turns out to be 8065 pounds. Consider now the following load ratios:

$$\bar{P}_{CR1} \Big/ \bar{\bar{P}}_{CR1} = 1.185$$

$$\bar{P}_{CR2} \Big/ \bar{\bar{P}}_{CR1} = 1.017 \qquad (13)$$

$$\bar{P}_{CR3} \Big/ \bar{\bar{P}}_{CR1} = 0.798$$

The correspondence between the ratios in Equations (12) and (13) strongly indicates that, in spite of the scatter among individual buckling loads for the small panels, the small and large panel data are self consistent in a gross, average sense. Therefore, each large panel and the small panels subsequently cut from it behave in the same relative way.

Another way of considering the above consistency issue is to construct the following ratios:

$$P_{CR1,1} \Big/ \bar{P}_{CR1} = 0.753$$

$$P_{CR1,2} \Big/ \bar{P}_{CR2} = 0.756 \qquad (14)$$

$$P_{CR1,3} \Big/ \bar{P}_{CR3} = 0.717$$

The closeness of the above ratios to each other indicates, perhaps even more convincingly, that the large and small panel data are self consistent. The theoretical value of the above ratio from the pretest design analysis is 0.612. The fact that the experimentally determined values are higher will be discussed subsequently.

The scatter reflected by the data in Table 7 should be greater than that of the data in Table 6 for the large parent panels. This is because the smaller

panels will be influenced to a greater degree by local manufacturing variations. The overall behavior of the small panels, on the basis of the arguments just presented, is quite intelligible.

The design analysis prediction of general instability for the panels as wide columns was based upon Equation (6), with the associated quantities defined in Equations (2), (3) and (7). The key geometric parameter is $\bar{I}$, the effective transformed moment of inertia per unit width of panel. In as much as control of the dimensions of the structural elements during manufacture, rib width in particular, has emerged as a matter that requires further investigation, it is important to explore what its influence may have been on the observed behavior of the panels. For this purpose, the mean dimensions in Table 5 are used. Also, assume that the ratio E_1/E_c is the same as used in the design analysis. Let $\bar{\bar{I}}$ denote the mean of calculated values of $\bar{I}$ for the large panels (1.096 $in.^3$). Then, consider the following ratios:

$$\begin{aligned} \bar{I}_1 \;/\; \bar{\bar{I}} &= 1.187 \\ \bar{I}_2 \;/\; \bar{\bar{I}} &= 1.032 \\ \bar{I}_3 \;/\; \bar{\bar{I}} &= 0.781 \end{aligned} \qquad (15)$$

The correspondence of these values with the loading ratios of Equations (12) and (13) is striking. It is not too bold a conjecture to attribute the observed differences in buckling behavior to geometric differences in the panels alone.

The correlation of relative buckling characteristics with available theory is obviously excellent. An absolute, quantitative comparison must await results from mechanical tests on elements taken from the panels and the determination of fiber and resin content.

Another issue requires attention. The ratios of second to first buckling loads given in Equations (11) are slightly low. Also, the ratios of the first buckling loads of the large to the small panels (Equations (14)) are somewhat

higher than the 0.612 value predicted by the design analysis. It appears that as the buckle wave length decreases (higher modes or shorter panels), the apparent stiffness of the panels is less than that predicted by the theory. One effect which has been neglected, but which exhibits this type of behavioral trend, is transverse shear deformation. It can be approximately accounted for with the equation

$$N_{CR} = \frac{N_E}{(1+N_E/S_Z)} \tag{16}$$

N_{CR}, as before, is the critical value of the stress resultant to cause buckling. N_E is critical value of the stress resultant according to engineering bending theory (the "Euler" value) which does not account for transverse shear deformation. S_Z is the transverse shear stiffness per unit width of panel.

For a uniform, homogeneous, isotropic panel, S_Z is determined from the following equation:

$$S_Z = k\ G\ t \tag{17}$$

k is a shear correction or shape factor, G is the shear modulus and t is the panel thickness. A correspondingly simple expression can be used for a CFACI panel. If it is assumed that the ratio of the shear modulus of the rib material, $G_{12,1}$, to that of skin, $G_{12,0}$, is the same as the corresponding Young's modulus ratio, then

$$S_Z = k\ (1+k_1\bar{\alpha})\ G_{12,0}t \tag{18}$$

In this equation, k_1 is a factor of order unity and t is the skin thickness. For the purpose of this discussion, k and k_1 have been set equal to unity in all calculations.

If Equations (16) and (18) and the mean dimensions from Table 5 are used to correct the theoretical predictions, the following ratios of second to first buckling loads are obtained:

$$P_{CR2,1}/P_{CR1,1} = 1.96$$
$$P_{CR2,2}/P_{CR1,2} = 1.97 \qquad (19)$$
$$P_{CR2,3}/P_{CR1,3} = 1.98$$

The correspondence of these values with those of Equations (11) determined from the experiments is excellent, therefore. Similar calculations of the ratios of large to small panel buckling loads give the following estimates:

$$P_{CR1,1}/\bar{P}_{CR1} = 0.712$$
$$P_{CR1,2}/\bar{P}_{CR2} = 0.705 \qquad (20)$$
$$P_{CR1,3}/\bar{P}_{CR3} = 0.695$$

Although not as close to Equations(14) as the above comparison, these predictions are the proper magnitude.

On the basis of the above considerations, it appears that transverse shear flexibility accounts for most of the observed departures from the (relative) predictions of engineering bending theory used in the design analysis. This is a reasonable conclusion as the rather low stiffness of the skin together with the unidirectional nature of the woven ribs results in a relatively low transverse shear stiffness.

One final matter has been explored in a limited way. In order to examine the applicability of smeared stiffener theory, three of the small panels, 1-1, 2-3, and 3-2, were trimmed to even smaller widths and compression tested. This trimming operation reduced the widths to approximately 3.50 inches, but, more importantly, reduced the number of backbone, lengthwise ribs from four to three. These three panels were selected because they buckled at higher loads than the other small panels from the corresponding parent panel sets. The data are presented in Table 8 in a manner that is convenient for comparison. Equal values of N_{CR} for both trimmed and untrimmed panels would correspond to the ideal situation. Evidently the portion removed from panel 1-1 corres-

ponds to a locally stiff zone as the critical stress resultant is reduced nearly 13 percent. Since the data indicate essentially no change for the remaining two panels, however, discrete stiffener effects are considered to be of second order and insignificant compared to manufacturing-related effects.

CONCLUDING REMARKS

CFACI is an attractive concept as it synergistically combines the efficiency of a stiffened structure with the superior specific strength and stiffness of an advanced composite in a manner that is compatible with automated manufacturing technology. The research described herein is the first attempt to evaluate it in load bearing structure. A data base has been established by the design, fabrication and test of flat panels as wide columns. Correlation of the experimental results with existing theory is, on a relative basis, excellent. A high degree of confidence can be held for absolute, quantitative correlation with theory after the completion of an element test program.

In summary, all of the objectives cited in the project overview have been met. Inconsistency in manufacturing has been clearly identified as the primary reason for the scatter of the test data. In a production environment, manufacturing variability poses no major problems, however; three pilot test articles hardly permit much progress in traversing the applicable learning curve. It has been learned that the critical dimension is rib width. Since geometry alone "explains" much of the observed behavior, it may even be possible to specify acceptance of a finished part in terms of rib width.

It has also been learned that transverse shear flexibility is an influence that cannot be ignored. An attempt to isolate its' influence will be a part of the element test program.

While a major step has been taken that inspires confidence in the use of CFACI, additional work must be done. The element tests are vitally important as strength as well as stiffness critical design conditions must be faced. Also, from the outset, the fabrication and evaluation of increasingly complex structural elements was planned. The circular cylindrical shells that have been designed should be fabricated and evaluated experimentally. The issue of imperfection sensitivity for this type of construction could then be explored.

ACKNOWLEDGMENTS

This work was supported by the United States Air Force Office of Scientific Research under contract F49620-77-C-0077. This support is gratefully acknowledged. Mr. William J. Walker has been the AFOSR program manager. Many individuals at McDonnell Douglas Astronautics-East have contributed in large and small ways to this project. The following people deserve special recognition:

J. Dutton
J. K. Lehman
R. A. Garrett
L. D. Mutchler
H. Lause
C. W. Neff
G. D. Renieri

Mr. Garrett provided overall supervision of the activity in St. Louis during most of the contract period. Mr. Lehman was responsible for the design analysis. Dr. Renieri and Mr. Lause were responsible for the manufacturing. Finally, Mr. A. D. Reddy, Graduate Research Assistant, School of Aerospace Engineering, was of enormous assistance during the test program.

REFERENCES

1. Isogrid Design Handbook, McDonnell Douglas Astronautics Company, Report MDC G4295A, February 1973.

2. Meyer, R. R., "Extension of Isogrid Manual to Materials With Different Moduli in Skin and Ribs", Internal Memorandum A3-250-ABCD-74-34, McDonnell Douglas Astronautics Company, April 1974.

3. Johnson, R., and Cohen, L.J., "Development of Graphite-Epoxy Isogrid Structure", presented at the 105th AIME Annual Meeting, February 22-26, 1976.

4. Peterson, J. P., "Buckling of Stiffened Cylinders in Axial Compression and Bending - A Review of Test Data", NASA TN D-5561, December 1969.

5. Various Authors, "Space Shuttle Isogrid Tank Buckling Test," Vol. I, Design and Analysis, McDonnell Douglas Astronautics Company, Report MDC G2804, February 1972.

6. Miller, R. J., "ORACLES: Orthotropic Analysis of Composites, Laminates and Elastic Structures", Douglas Aircraft Company, Report SM-47852, April 1965.

7. Allen, P. W., Lindley, P. B., and Payne, R. A., Use of Rubber in Engineering, Maclaren and Sons, London, 1967.

8. Cremens, W. S., "Manufacturing Methods for Thermal Expansion Molding of Advanced Composite Aircraft Structures", AFML-TR-75-110, 1975.

9. Horton, W. H., Cundari, F. L., and Johnson, R. W., "Applicability of the Southwell Plot to the Interpretation of Test Data Obtained From Stability Studies of Elastic Column and Plate Structures", USAAVLABS Technical Report 69-32, November 1971.

10. Jones, R. E., and Greene, B. E., "Force/Stiffness Technique for Nondestructive Buckling Testing", Journal of Aircraft, Vol. 13, No. 4, April 1976, pp. 262-269.